Deltaic deposits at Aeolis Dorsa: Sedimentary evidence for a standing body of water on the northern plains of Mars

Roman A. DiBiase,[1] Ajay B. Limaye,[1] Joel S. Scheingross,[1] Woodward W. Fischer,[1] and Michael P. Lamb[1]

[1]   A fundamental long-standing question regarding Mars history is whether the flat and low-lying northern plains ever hosted an ocean. The best opportunity to solve this problem is provided by stratigraphic observations of sedimentary deposits onlapping the crustal dichotomy. Here, we use high-resolution imagery and topography to analyze a branching network of inverted channel and channel lobe deposits in the Aeolis Dorsa region, just north of the dichotomy boundary. Observations of stacked, cross-cutting channel bodies and stratal geometries indicate that these landforms represent exhumed distributary channel deposits. Observations of depositional trunk feeder channel bodies, a lack of evidence for past topographic confinement, channel avulsions at similar elevations, and the presence of a strong break in dip slope between topset and foreset beds suggest that this distributary system was most likely a delta, rather than an alluvial fan or submarine fan. Sediment transport calculations using both measured and derived channel geometries indicate a minimum delta deposition time on the order of 400 years. The location of this delta within a thick and widespread clastic wedge abutting the crustal dichotomy boundary, unconfined by any observable craters, suggests a standing body of water potentially $10^5 \, \text{km}^2$ in extent or greater and is spatially consistent with hypotheses for a northern ocean.

Citation: DiBiase, R. A., A. B. Limaye, J. S. Scheingross, W. W. Fischer, and M. P. Lamb (2013), Deltaic deposits at Aeolis Dorsa: Sedimentary evidence for a standing body of water on the northern plains of Mars, *J. Geophys. Res. Planets*, *118*, 1285-1302, doi:10.1002/jgre.20100.

1.   Introduction

[2]   The former extent and stability of liquid water on the surface of Mars constitute fundamental problems in understanding its planetary evolution. It remains unclear whether the planet was ever much warmer or wetter than today [*Carr*, 1996]. While there is extensive evidence for landforms sculpted by flowing water (e.g., incised valley networks, streamlined islands, and cutoff meanders [*Baker and Milton*, 1974; *Sharp and Malin*, 1975; *Carr*, 1996; *Craddock and Howard*, 2002]), it is challenging for early Mars climate models to sustain clement mean annual surface temperatures primarily due to lower solar luminosity earlier in Mars' history, though the boundary conditions for these models are poorly constrained [e.g., *Sagan and Mullen*, 1972; *Haberle*, 1998]. A similar problem exists concerning climate and surface processes on the early Earth, and ultimately it has been observations of sedimentary rocks in the terrestrial geological record that demonstrate that Earth's oceans are long-lived features and provide the first-order insight into the history of Earth's water budget [e.g., *Van Kranendonk*, 2006]. The same logic applies to Mars [e.g., *Malin and Edgett*, 2000; *Grotzinger et al.*, 2005], and with limited lander and rover observations, we must rely more heavily on orbital remote sensing data. A strong debate surrounds sedimentary and geomorphological observations for standing bodies of water on the surface of Mars, either in the form of crater lakes [*Newsom et al.*, 1996; *Cabrol and Grin*, 1999; *Fassett and Head*, 2008; *Buhler et al.*, 2011; *Goudge et al.*, 2012], or more provocatively as a hemispheric ocean spanning the northern lowlands [*Parker et al.*, 1989; *Baker et al.*, 1991]. These issues can be greatly informed with more detailed observations of Mars' sedimentary record, enabled by the growing amount of high-resolution imagery being sent back to Earth (e.g., Mars Orbiter Camera (MOC) [*Malin and Edgett*, 2001], High-Resolution Imaging Science Experiment (HiRISE) [*McEwen et al.*, 2007], and Context Camera (CTX) [*Malin et al.*, 2007]).

[3]   At a global scale, the crustal dichotomy of an elevated, cratered, and dissected southern hemisphere versus the relatively smooth northern lowlands has long hinted at the possibility of a former northern ocean, the presence of which would have profound implications for the early climate and habitability of Mars [*Sharp*, 1973; *Lucchitta et al.*, 1986; *Head et al.*, 1999; *Aharonson et al.*, 2001; *Perron et al.*,

---

[1]Division of Geological and Planetary Sciences, California Institute of Technology, Pasadena, California, USA.

Corresponding author: R. A. DiBiase, Division of Geological and Planetary Sciences, California Institute of Technology, 1200 E. California Blvd., Pasadena, CA 91125, USA. (rdibiase@caltech.edu)

2007]. Early workers argued for a northern ocean based on the presence of inferred shoreline features (i.e., the Arabia shoreline of *Parker et al.*, [1993]) and the location of large outflow channel mouths along the dichotomy boundary [*Ivanov and Head*, 2001]. However, more detailed examinations of these proposed shoreline features with MOC imagery failed to provide clear morphologic evidence of wave-cut benches, spits, and other distinctive landforms commonly used to mark paleoshorelines on Earth [*Malin and Edgett*, 1999; *Ghatan and Zimbelman*, 2006]. In addition, under the assumption that a northern ocean would likely be of Late Hesperian age or older [*Fairen et al.*, 2003], it is questionable whether the subtle (O(1–10 m)) morphologic signatures of shoreline features would be preserved following more than one billion years of aeolian surface modification [*Irwin and Zimbelman*, 2012]. Because of resurfacing due to impacts, volcanism, and ongoing aeolian (and perhaps occasionally fluvial) erosion and deposition, current Mars topography provides an imperfect record of its environmental history. However, although shorelines and associated geomorphological features are rarely preserved over long timescales, similar information (i.e., paleoenvironment) can be gleaned from the nature and distribution of sedimentary deposits.

[4] Based on surface morphology alone, it is difficult to determine the processes responsible for creating distinct depositional features. For example, *Malin and Edgett* [2003] and *Moore et al.* [2003] described a well-preserved, fan-shaped deposit in Eberswalde crater that they argued was built by fluvial processes based on the presence of meander cutoffs, scroll bars, and other distinctive landforms preserved within the strata, resolved by MOC images. *Jerolmack et al.* [2004] interpreted these deposits as an alluvial fan, and used measurements of surface slope and channel width combined with scaling factors typical of terrestrial analogs to estimate the total discharge necessary to build the observed topography, estimating a minimum formation timescale of order 100 years. In contrast, *Bhattacharya et al.* [2005] and *Wood* [2006] used the surface morphology of multiple discrete depositional lobes to infer a deltaic origin for the Eberswalde deposits, with the implication that the crater may have once been substantially filled by a standing body of water. Incorporating stratigraphic evidence in addition to surface morphology enables a more detailed discrimination of processes. *Lewis and Aharonso*n [2006] measured the attitude of bedding planes within the deposits at Eberswalde and found roughly uniformly dipping beds at ~2°, which they interpreted as the low-angle topsets of an aggradational delta whose more steeply dipping foresets have been eroded away. However, because the distinguishing sedimentary evidence for a delta (i.e., steep foresets) is missing at Eberswalde, both the alluvial fan and delta interpretations are plausible, and consequently robust evidence for a long-standing body of water in Eberswalde crater remains ambiguous given current observations.

[5] Similar studies of fan-shaped deposits at Jezero crater [*Fassett and Head*, 2005; *Ehlmann et al.*, 2008; *Schon et al.*, 2012] and Melas Chasma [*Metz et al.*, 2009] provide more convincing evidence of long-lived lacustrine environments. At Jezero crater, the combination of an upstream, well-developed tributary valley network, well-preserved lobate deposits at the crater inlet, and a meandering outflow channel suggests that fan-deposits grew steadily within a stable crater-lake

system rather than in pulses of accumulation following large outburst flood events [*Schon et al.*, 2012]. At Melas Chasma within Valles Marineris, elongated depositional lobe geometries, consistently low dip magnitudes (~1°), and remoteness from inferred paleoshorelines led *Metz et al.* [2009] to infer a sublacustrine origin for the deposits, drawing analogy to the Mississippi River submarine fan, U.S.A.

[6] These three examples (Eberswalde, Jezero, and Melas) highlight the necessity of incorporating stratigraphic, in addition to morphologic, analysis when interpreting deposits on Mars. Specifically, the current topographic forms of these deposits may bear little resemblance to the original depositional surfaces, and the steep toes commonly interpreted to be deltaic foresets may instead be erosional, as is inferred by both the alluvial fan [*Jerolmack et al.*, 2004] and delta [*Lewis and Aharonson*, 2006] interpretations of the deposits at Eberswalde, and the delta deposits at Jezero [*Schon et al.*, 2012]. Yet, while the above examples have implications for local hydrology [e.g., *Newsom et al.*, 1996], it is not clear whether they have a direct bearing on the global-scale water budget. The limited extent of these deposits (O(1 km)), their local topographic confinement in craters with diameters on the order of 10 km, and their direct connection to preserved upstream valley networks may instead correspond to localized late-stage fluvial activity [*Mangold et al.*, 2012].

[7] Terby crater, along the northern margin of the Hellas Basin, contains an extensive layered sedimentary deposit, now partially exhumed, that serves as an example where stratigraphic analysis reveals critical information about depositional environment that is absent in the analysis of present morphology. Here, *Ansan et al.* [2011] mapped a deltaic sequence with nearly 2 km of section exposed, including clinoforms, visible truncations, unconformities, and spectral signatures consistent with the presence of hydrated minerals. Despite the extent of the deposits at Terby crater, the upstream source of water and sediment is absent, presumably due to erosion since Noachian time [*Ansan et al.*, 2011]. The preserved strata in Terby crater thus provide an important record of the history of fluvial-lacustrine activity over a large portion of Mars history in the northern Hellas Basin.

[8] Discovery of deltaic or subaqueous deposits in the northern lowlands would strengthen the evidence for a hemispheric ocean. Recently, *Di Achille and Hynek* [2010] compiled a database of 52 putative deltas that cluster within a few hundred kilometers of the crustal dichotomy. Of these, 17 deltas are connected to the northern lowlands (i.e., not located within closed crater basins) and lie along an equipotential surface of −2540 ± 177 m elevation, closely matching the mean trend of the inferred Arabia shoreline [*Clifford and Parker*, 2001; *Di Achille and Hynek*, 2010]. In principle, the identification of deltaic deposits along this boundary provides strong sedimentary evidence of a northern ocean. However, the criteria used by *Di Achille and Hynek* [2010] to identify deltas rely heavily on morphologic evidence such as the presence of a steep front; in some cases, the observed front may be erosional and may not necessarily indicate steeply dipping strata (i.e., foreset beds) [e.g., *Lewis and Aharonson*, 2006]. Additionally, the *Di Achille and Hynek* [2010] database includes many examples of fan-shaped deposits at the outlets of incised valley systems. In these settings, deposition is more likely to have been driven by spatial changes in topographic confinement, as occurs for alluvial and debris flow fans, rather
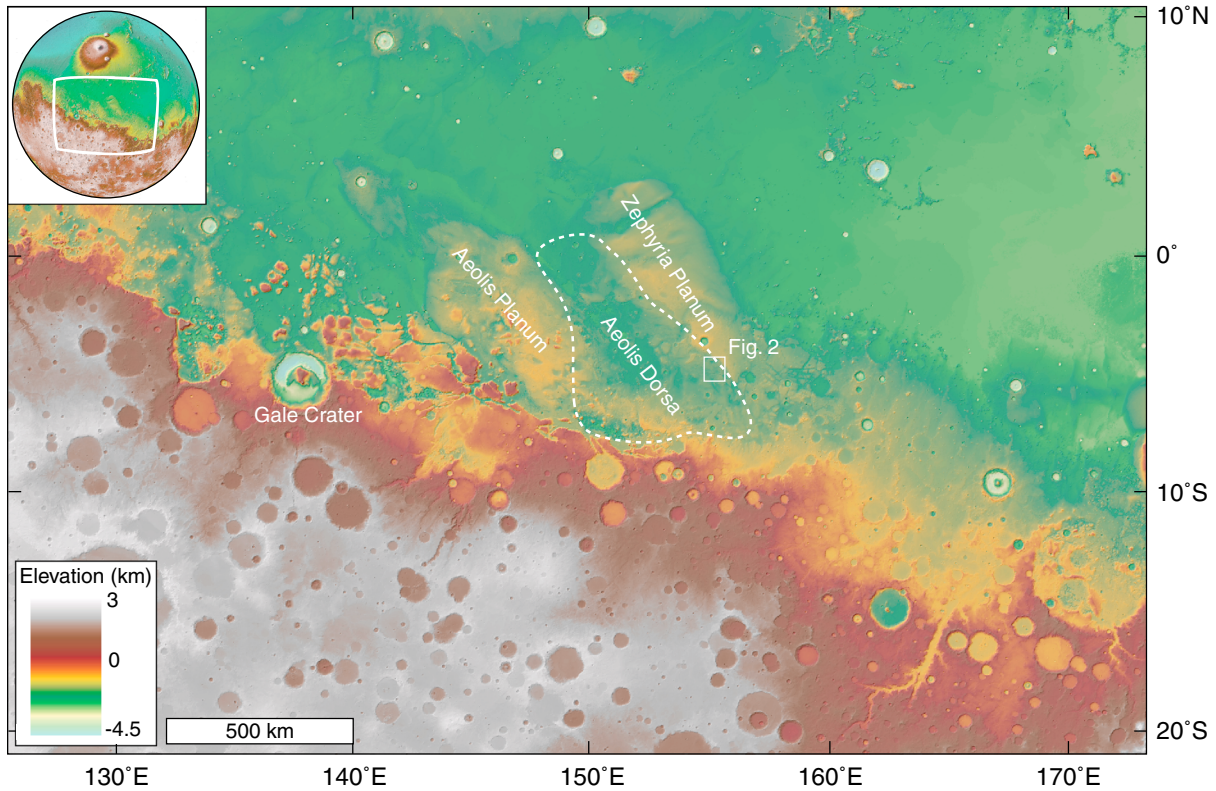
Figure 1. Overview map of the Aeolis Dorsa region. An erosional window into underlying deposits reveals the extensive distribution of sedimentary deposits with common inverted channel features (dashed outline), positioned just north of the crustal dichotomy. White box outlines extent of Figure 2.

than by debouchment into a standing body of water [*Blair and McPherson*, 2009]. It is clear that observations of deposit stratigraphy in the region of the Northern Plains are needed to test the hemispheric ocean hypothesis.

[9] In this contribution, we employ a combination of high-resolution (0.25 and 5–6 m) satellite images (HiRISE and CTX) and associated stereophotogrammetric digital elevation models (DEMs) (1 and 18 m resolution from HiRISE and CTX, respectively) to quantify the stratigraphic architecture of a thick sedimentary succession containing a complex interbedded network of channels within the stratigraphy. Our study area lies just north of the dichotomy boundary at the southeastern edge of Aeolis Dorsa and covers a small portion of a much broader deposit with abundant inverted channel features spanning an area of over 10^5 km² [*Burr et al.*, 2009, 2010; *Lefort et al.*, 2012]. We use crosscutting relationships of depositional channel and lobe features, the geometry of individual channel elements and bed thicknesses, and the attitude of stratigraphic bedding from high-resolution topography to evaluate the stratigraphic architecture of the deposit and infer both paleoflow direction and depositional environment (e.g., tributary network, alluvial fan, submarine fan, or shoreline delta). Finally, we apply common scaling relationships and geometrical arguments based on terrestrial analogs to estimate water and sediment fluxes and the total time recorded by the deposits. Altogether these observations provide a new level of support for hypotheses positing an ancient hemispheric ocean in the northern lowland basin of Mars.

2. Aeolis Dorsa: Geologic Setting and Prior Work

2.1. Medusae Fossae Formation

[10] The Medusae Fossae Formation (MFF) is an extensive layered deposit onlapping the crustal dichotomy from 140° to 230°E longitude, and in places reaching thicknesses of 2–3 km [*Scott and Tanaka*, 1986; *Greeley and Guest*, 1987]. While there has been considerable debate over its origin, the current leading hypothesis is that the MFF is analogous to large terrestrial ignimbrite deposits based on unit-wide layering, its proximity to the volcanic center of Apollinaris Patera, and the morphology of ubiquitous yardangs [*Mandt et al.*, 2008; *Zimbelman and Griffin*, 2010; *Kerber et al.*, 2011]. Subsurface investigations of the MFF from radar soundings (Mars Advanced Radar for Subsurface and Ionospheric Sounding–MARSIS, and Shallow Subsurface Radar–SHARAD) confirm that the MFF drapes the dichotomy boundary and reveal low permittivity that is consistent with a wide range of lithologies including low density sedimentary and pyroclastic deposits [*Watters et al.*, 2007; *Carter et al.*, 2009; *Mouginot et al.*, 2010; *Mouginot et al.*, 2012]. Complicated stratigraphic relationships with Amazonian Cerberus lavas and difficulties in crater counting associated with the friable nature of the MFF have led to conflicting age estimates. While initially interpreted to be of middle Amazonian age based on a lack of preserved craters, updated crater counting analyses suggest the lower MFF is late Hesperian in age or older and the low crater density reflects an exhumation, rather than emplacement age [*Kerber and Head*, 2010; *Zimbelman and Scheidt*, 2012].
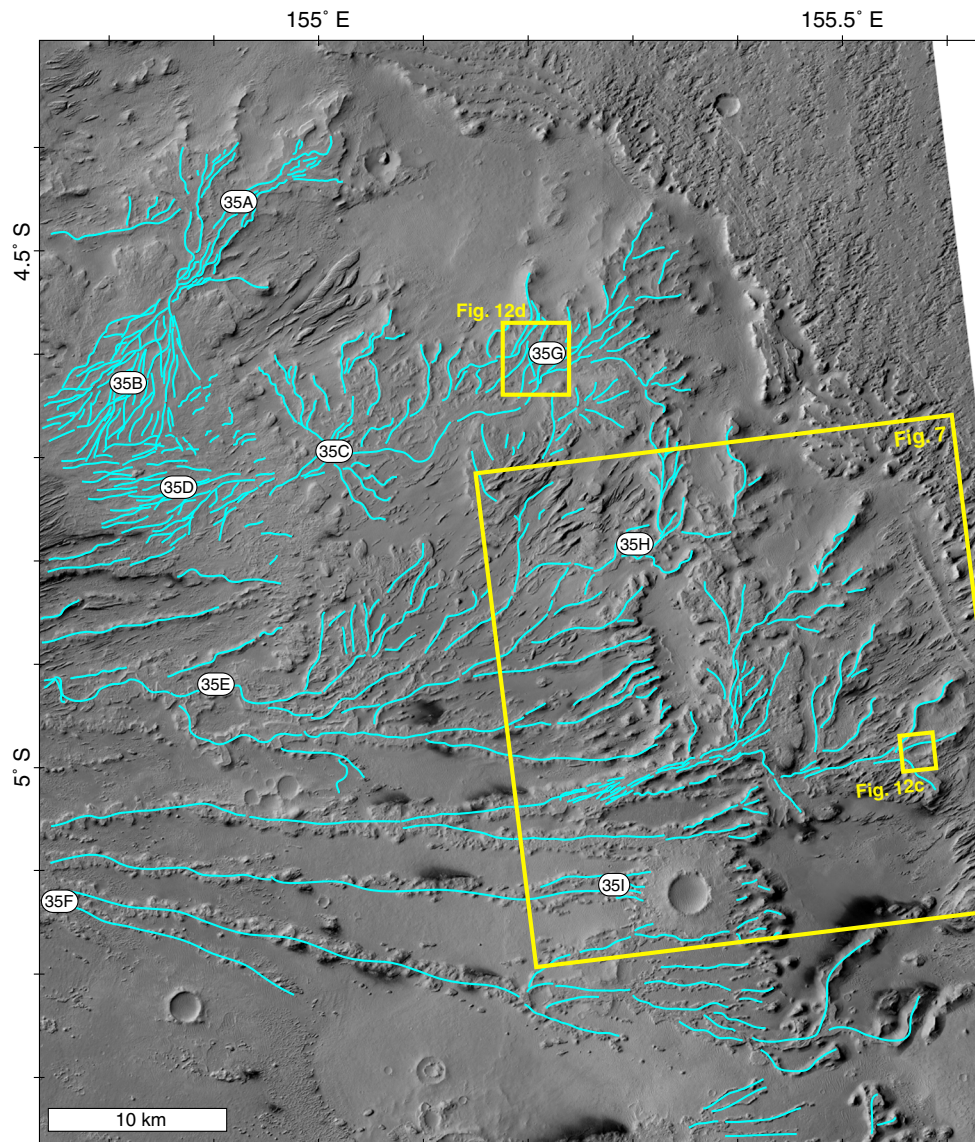
Figure 2. Regional map showing distribution of inferred inverted channels (blue) on top of CTX imagery. Circles refer to site numbers from *Burr et al.* [2009]. Yellow boxes indicate extents of Figure 7 and Figures 12c and 12d.

2.2. Sinuous Ridges at Aeolis Dorsa

[11] The lower MFF in the Aeolis Dorsa region, between Aeolis and Zephyria Plana (Figure 1), contains the highest concentration of mapped "sinuous ridges" on Mars [*Burr et al.*, 2009]. These sinuous ridges encompass a wide range of morphologies, including wispy, discontinuous low relief features; narrow, highly sinuous individual ridgelines; and lobate, flat-topped platforms. *Burr et al.* [2009] mapped the distribution of sinuous ridges at Aeolis Dorsa and interpreted them as representing the inverted topography of former fluvial channels. On Mars, inverted topography is typically interpreted to be a result of enhanced erosional resistance of channel deposits due to lava infill, chemical cementation, or coarse sediment armoring [e.g., *Pain et al.*, 2007; *Williams et al.*, 2009; *Newsom et al.*, 2010]. Sinuous ridges may also reflect coarse sediment lags of subglacial channels (eskers). *Burr et al.*

[2009, 2010] discussed these mechanisms in detail with regard to the deposits at Aeolis Dorsa and argued that lava and esker origins can be ruled out for all but a minor subset of the deposits based on their cross-sectional and planform geometries. Rather, abundant observations of scroll bars, cutoff meanders, and fine stratigraphic layering points to an origin as fluvial deposits derived from meandering and braided rivers [*Burr et al.*, 2009, 2010].

[12] A more difficult question lies in interpreting the timing and paleoenvironment of the fluvial activity. While there are many examples of yardang-rich deposits (without clear channel features) overlying inverted channels, suggesting that the channels are confined to the lower member of the MFF [*Zimbelman and Griffin*, 2010], their stratigraphic relationship with the putative ignimbrite deposits elsewhere in the MFF is unclear. Do the inverted channels of Aeolis Dorsa represent local fluvial reworking of the lower MFF volcanic deposits, or
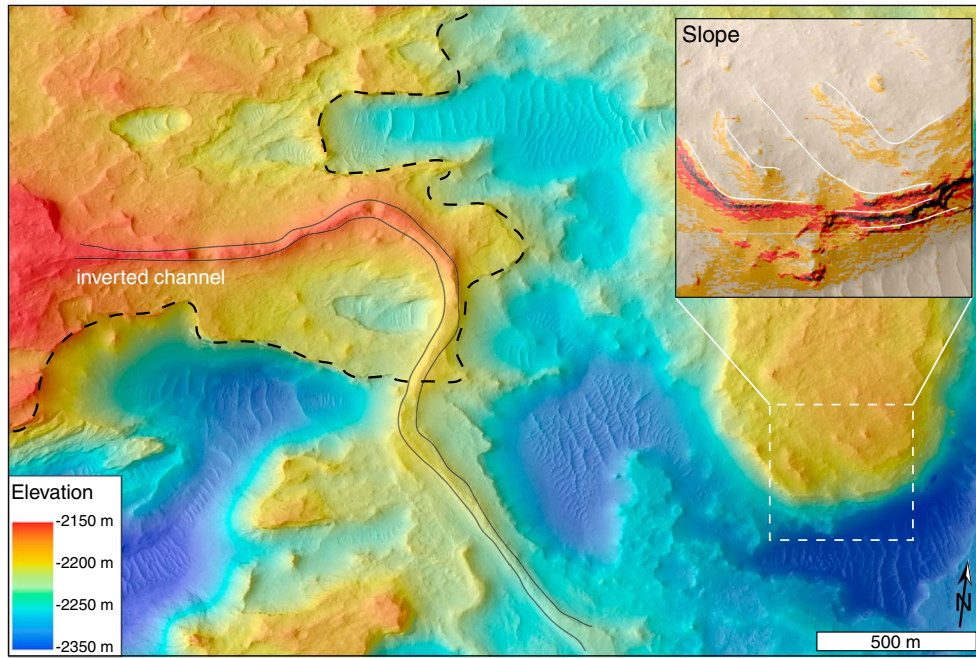
Figure 3. Overlay of HiRISE digital elevation model over HiRISE imagery, highlighting the morphological expression of inverted channel elements, elevated channel complex (dashed line), and exposed stratigraphic bedding planes (white lines, inset), dipping ~4° to the southeast, and interpreted as delta foresets. Inset shows slope map (tan = 0–25°; orange = 25–35°; red = 35–45°; black = 45–90°) of exposed bedding planes used to aid in picking elevation points to measure bedding attitudes.

do they form the upper surface of an older clastic sedimentary sequence? Ultimately, these end-member cases depend on whether the inverted channels represent a drainage network on a coeval geomorphic surface or channel bodies within a sedimentary deposit constructed by fluvial processes. Southeastern Aeolis Dorsa (Figure 2) presents perhaps the best opportunity to address these questions, due to the high density of inverted channels and preserved networks of channels. The current hypothesis for this region, based primarily on regional topography that dips to the west, is that these channels (blue lines in Figure 2) represent a preserved convergent paleodrainage network flowing from east to west [*Burr et al.*, 2009; *Lefort et al.*, 2012]. Here, we build on this work by analyzing in detail the morphologic and stratigraphic evidence for paleoflow direction and depositional setting, ultimately favoring the interpretation that these channels elements are part and parcel of a thick clastic sedimentary deposit from a distributary network with paleoflow to the east.

3. Stratigraphic Analysis of a Branching Channel Network

3.1. DEM Generation

[13] We focused our attention on a well-preserved branching network of inverted channel bodies currently being exhumed by the removal of younger units of the MFF at the eastern edge of Aeolis Dorsa, analyzing the overlap extent of CTX images G03_019328_1750_XN_05S204W and G04_019961_1750_XN_05S204W (yellow box, Figure 2). The central portion of our study area is additionally covered by the HiRISE stereo pair ESP_019328_1750 and ESP_019961_1750. We generated two DEMs, with grid

resolutions of 1 m for the HiRISE pair and 18 m for the CTX pair, using common stereogrammetry methods [*Kirk et al.*, 2008; *Lewis et al.*, 2008; *Limaye et al.*, 2012]. We processed images with USGS ISIS 3 software and derived DEMs using BAE Systems' SOCET SET. The elevation of ground control points used for both DEMs was provided by data from the Mars Orbiter Laser Altimeter, which has a vertical accuracy of ~1 m and a surface spot size of ~168 m in mapping orbit [*Smith et al.*, 2001]. Consequently, we picked control points on areas of low topographic relief and avoided steep slopes. The vertical precision of the photogrammetry techniques applied here is approximately 0.5 m and 10 m for the HiRISE and CTX DEMs, respectively. This precision varies as a function of viewing orientation, image resolution, and pixel-correlation error [*Kirk et al.*, 2008; *Fishbaugh et al.*, 2010; *Okubo*, 2010].

3.2. Morphologic and Stratigraphic Analysis

[14] We used the DEM and imagery data to map in detail the distribution of inverted paleochannels and channel complexes. We use the term paleochannel to refer to ribbon channel bodies that may reflect original channel dimensions and channel complex to refer to broad amalgamations of channels that are analogous to meander-channel belts [e.g., *Gibling*, 2006]. We map channel complexes by searching for relatively planar surfaces that protrude (i.e., were inverted from) from the surrounding topography and show evidence of sedimentary layering (Figure 3). These surfaces are generally free of surficial yardangs and sand dunes, and many of the surfaces are mantled by smaller-scale sinuous ridges that we interpret as the partially preserved traces of individual paleochannels. To aid in identifying features such as
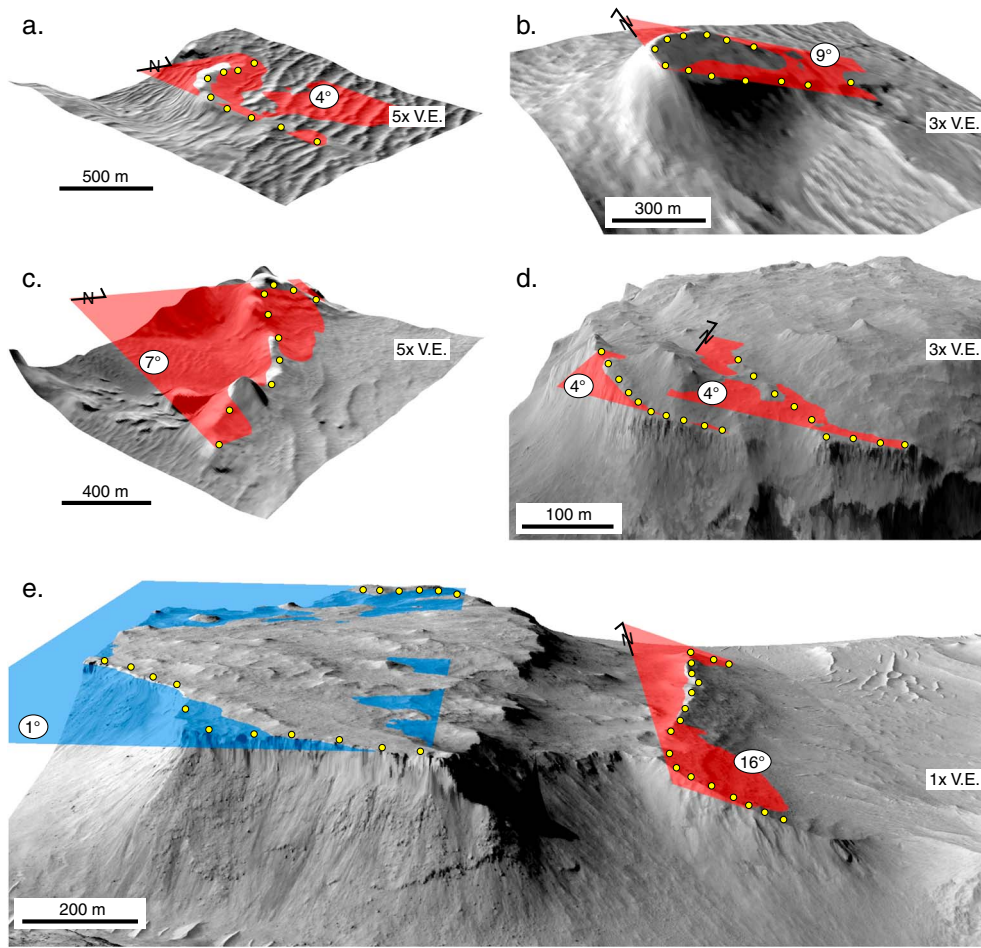
Figure 4. Dip measurement examples showing fitted planes and perspective imagery views (a–c) CTX and (d, e) HiRISE. Dotted lines highlight edges of inferred bedding planes. Blue plane in Figure 4e is based on the top of a continuous caprock surface (see Figure 6 for further examples) and dips to the NE. Vertical exaggeration (V.E.) ranges from 1 to 5x.

paleochannels and bedding planes, we generated a slope map from the HiRISE DEM by calculating the dip of a plane fit through a 3×3 m window at each pixel (Figure 3 inset). We visually identified sharp breaks in slope separating the channel complex top from the surrounding topography and used these slope breaks to mark the channel complex boundaries (dashed line, Figure 3). We excluded areas that appear to have been modified by large craters or by the deposition of impact ejecta.

[15] Within the mapped deposits, we used CTX and HiRISE imagery to identify exposed stratigraphic planes where we could characterize bed geometry (i.e., strike and dip). We focused on areas where bedding planes were laterally extensive and visible in the topographic data: ~100 m for areas covered by HiRISE topography and ~1 km for areas covered only by CTX data. Additionally, we sought exposures with significant planform curvature in order to better constrain plane fits. For each exposure, we selected 10–50 points based on visual examination of imagery and topographic data. We extracted coordinates and elevations for each point and fit a plane through the data using ordinary linear-least squares regression. Fit uncertainties based on the attitude of the plane-normal vector range from 0.5° to 2° at the 95% confidence level. To assess the quality of fits in a geologic context (i.e., interpret whether the identified

planar features are bedding planes), we isolated each feature and rendered the fitted plane and the imagery draped over the DEM in 3D perspective (Figure 4).

[16] In addition to measuring bed orientation, we also used the HiRISE DEM to analyze the morphology of inverted paleochannels and channel complexes (Figure 5). Many of the channel complexes preserved within our study area feature a locally resistant caprock unit that supports their topographic inversion. We used this caprock layer as a proxy for paleochannel flow depth (see section 6), as well as for low-angle bedding plane geometry, which is otherwise difficult to quantify on the low-relief, but locally rough, surface of inverted channel complexes. The caprock forms a butte and is expressed prominently in the HiRISE DEM by regions with local side slopes steeper than 45°. For over 300 locations within the extent of the HiRISE DEM (including the main trunk channel complex and parallel channel complex features to the south), we extracted the elevations of both the top and bottom of the exposed caprock using local topographic profiles to highlight slope breaks. For a subset of exposures along a main trunk channel complex (Figure 6a), we projected the elevations of the upper and lower caprock boundaries into the strike of inferred flow direction (approximately E-W) and estimated apparent dip magnitudes.
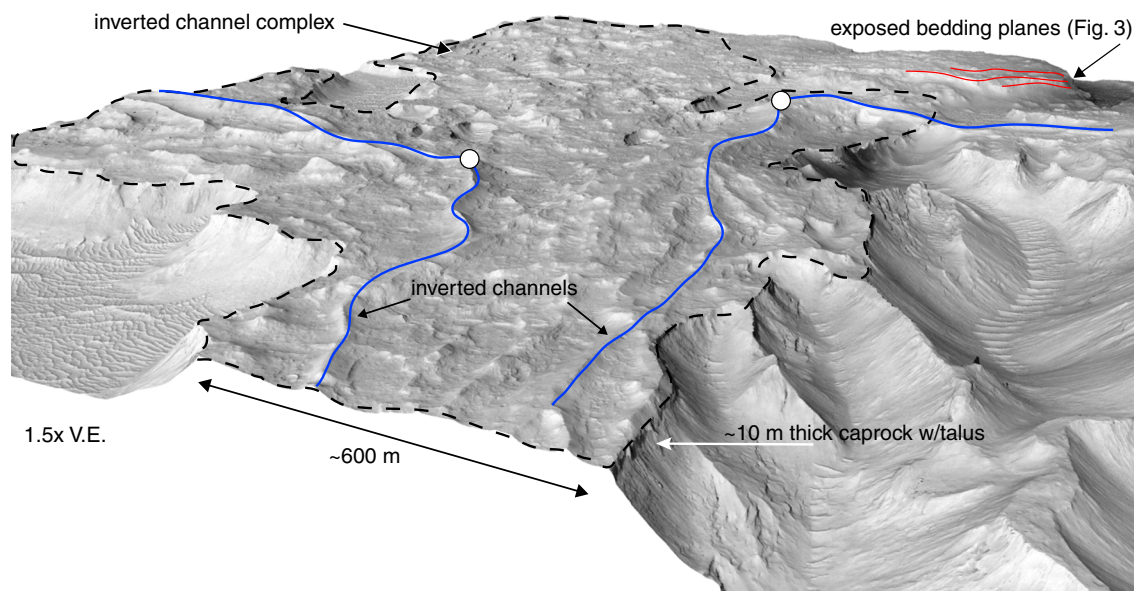
Figure 5. Perspective view of an inverted channel complex (dashed outline) showing HiRISE imagery draped over HiRISE topography. Relief of the channel complex relative to surrounding topography is ~100 m, while relief of individual channel elements (e.g., blue lines) is on the order of 10 m. Red lines indicate stratigraphic bedding planes shown in Figure 3. Circles mark the location of relatively sharp channel turns on different elements within the complex. These are located at approximately the same elevation, -2200 m, which implies a base-level control on channel avulsion.

4. Geologic Mapping Results

[17] The results of our geologic and stratigraphic mapping are highlighted in Figure 7, which shows the topography (Figure 7a), distribution of inverted channel complexes (Figure 7b), and inferred superposition of depositional lobes (Figure 7c). Inverted channel complexes are typically on the order of 1 km across, raised ~100 m above surrounding topography and capped by a 10–30 m thick resistant caprock layer that forms near-vertical slopes (Figures 5 and 6). Where preserved, individual inverted paleochannels are approximately 50–100 m wide and raised 10–20 m above the surface of the raised channel complexes (Figures 3, 5, and 6). In two locations, well-preserved inverted paleochannels diverge and drop ~100 m in elevation to the east (stars in Figure 7c [*Lefort et al.*, 2012, Figure 9]). Most individual paleochannels, however, are discontinuous and are difficult to trace for distances greater than a few kilometers. On the main trunk channel complex, two paleochannels make abrupt turns at similar elevations, highlighted by circles in Figures 5 and 6. At a broader scale, the mapped depositional lobes lie at similarly sharp angles to the trunk channel complex (Figure 7c).

[18] Measurements of stratigraphic bedding plane orientations show dips ranging from 4 to 16°, with dip directions fanning generally to the east (Figure 7c). Accurate measurements of bedding planes on the trunk channel complex are difficult due to low topographic relief, although extensive near-horizontal layering is observed throughout its length (Figure 8 inset). Instead, we used the exposure of a resistant caprock at the top of the main trunk channel complex as a proxy for bedding attitude. We interpret this caprock as a fundamental component of the stratigraphic architecture based on bedding features visible in HiRISE images and thus use its bounding contacts as estimates of stratal geometry.

Measurements of caprock thickness taken regionally show a gradual thickening from <10 m in the west to ~30 m in the east (Figure 9), and we used both the upper and lower traces of this unit to estimate stratal geometries. At the west end, both the upper and lower traces of the caprock dip approximately 0.5° to the east, which is within the error of the measurement technique, and we interpret this as indicating a comparably low depositional slope (Figure 6c). Downstream, there is a subtle slope break in both trends that corresponds with the location of prominent paleochannel and channel complex switches where the caprock steepens to 3° (Figure 6). To the south of the main trunk channel complex is an even clearer example, where a low-angle caprock unit nearly abuts a prominent bedding plane dipping steeply (16°) to the east (Figure 4e).

5. Stratigraphic Interpretations, Basin Orientation, and Depositional Environments

5.1. Reconciling Modern Topography and Stratal Geometry

[19] Inverted channels on Earth and Mars can provide a window into past environmental conditions that are otherwise difficult or impossible to reconstruct. However, it is important to be aware of potential pitfalls when attempting to extract channel geometries, surface slopes, and paleoflow directions. For example, topographic profiles taken from the tops of inverted channels may not reflect paleochannel slopes for a number of reasons, including differential erosion or postdepositional deformation due to differential settling, or tectonism [*Lefort et al.*, 2012]. In many cases, individual paleochannels are not continuously preserved, and inferred paleochannel profiles may connect discordant features. At
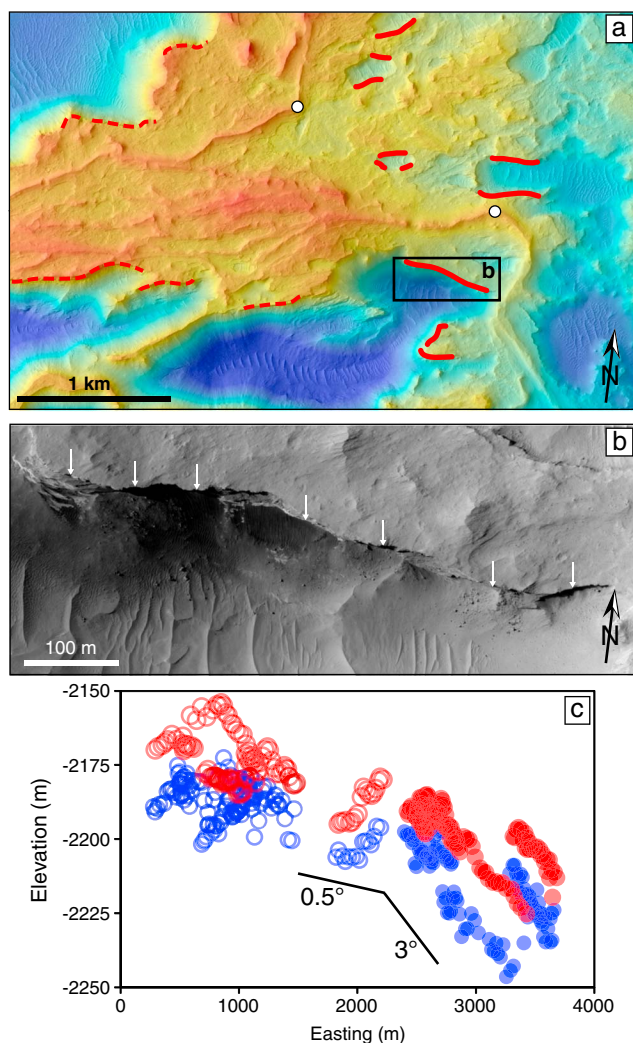
Figure 6. Channel body attitude estimated from the orientation the resistant cap rock. (a) Map of vertical caprock extent (red lines) on top of HiRISE topography and imagery. Elevation scale is the same as Figure 3, and circles indicate channel turns highlighted in Figure 5. (b) HiRISE imagery showing detailed morphology of resistant caprock layer (arrows). Illumination is from the NW. (c) Plot of elevation versus easting for top (red) and bottom (blue) of near-vertical caprock layer. Open symbols highlight gently dipping caprock (dashed lines in Figure 6a), while solid symbols indicate more steeply dipping caprock segments (solid lines in Figure 6a), interpreted as delta foresets.

Aeolis Dorsa, clear stratigraphic relationships between deposits with inverted channels and yardang-bearing units from the overlying MFF suggest significant burial and subsequent exhumation of channel deposits, and regional trends in modern topography likely do not represent a coeval paleogeomorphic surface. Additionally, the exposed strata from which we make our dip measurements (Figure 4) clearly indicate that the current topography is not a paleogeomorphic surface. However, observations of continuous, well-preserved inverted paleochannels whose width and relief stay relatively constant provide occasional instances where topographic profiles are minimally affected by

differential erosion. An example of this is shown in Figure 3, where an inverted paleochannel with 10–20 m of relief drops ~100 m across a topographic break to the east. Because the elevation drop is several times greater than the thickness of the channel deposit, it is unlikely that the modern topographic profile is due to differential erosion [*Lefort et al.*, 2012], and therefore here an actual step in the paleotopography is plausible. Thus, this feature either indicates flow to the east or is a result of short-wavelength (<1 km) postdepositional deformation. For most channel features, however, differential erosion cannot be ruled out, and we focus instead on stratal geometries, which are insensitive to erosion, rather than modern topography.

[20] While stratal geometries are unaffected by differential erosion, they may be influenced by postdepositional deformation associated with differential settling or tectonic processes. Although there is no clear evidence for faulting in our study area, *Lefort et al.* [2012] showed that this region is characterized by broad west-east topographic undulations with wavelengths of 20–50 km and amplitudes of 100–200 m. As a result, we are cautious in our interpretation of absolute dip magnitudes, especially for features with dips less than ~1°. The spatial pattern and relative stratal geometries over wavelengths shorter than ~20 km are probably not affected by deformation [*Lefort et al.*, 2012], however. For example, we observe a break in dip-slope from nearly flat to east-dipping beds (e.g., Figures 4e and 6c) in multiple areas. Because these changes in the slope of bedding planes occur over short distances (<1 km), and are furthermore associated with the planform changes in the deposit (e.g., a change from channelized to lobate morphologies), we interpret the breaks as primary features of the stratigraphic architecture. Thus, we assume that regional deformation in our study area has not significantly affected the stratal geometries (likely less than 1°), and due to the high likelihood for differential erosion (e.g., Figure 8), we rely on stratal geometries rather than modern topography except where paleotopographic change can be inferred as significant, as discussed above.

5.2. Mechanisms of Topographic Inversion and Implications for Paleoflow Direction

[21] The interpretation of paleodepositional environment at Aeolis Dorsa depends on the presumed mechanism of topographic inversion. To highlight this, we consider two end-member conceptual models: one in which an original, temporally concurrent channel drainage network is preserved, and another where the exhumation of a deposit leaves multiple channel complexes (that need not have been concurrent) at the surface.

[22] In the first case, which we describe as "landscape inversion," differential erosion of channel deposits and hillslope materials leads to the preservation of an original, temporally concurrent channel network elevated above the surrounding topography (Figure 10a). For terrestrial examples, the increase in erosional resistance of channel material is typically due to preferential cementation or duricrust formation in coarser and/or more porous alluvium [e.g., *Pain and Ollier*, 1995], or from lava-infill [e.g., *Rhodes*, 1980] (Figures 10a,11a, and 11b). As a result, a coeval geomorphic
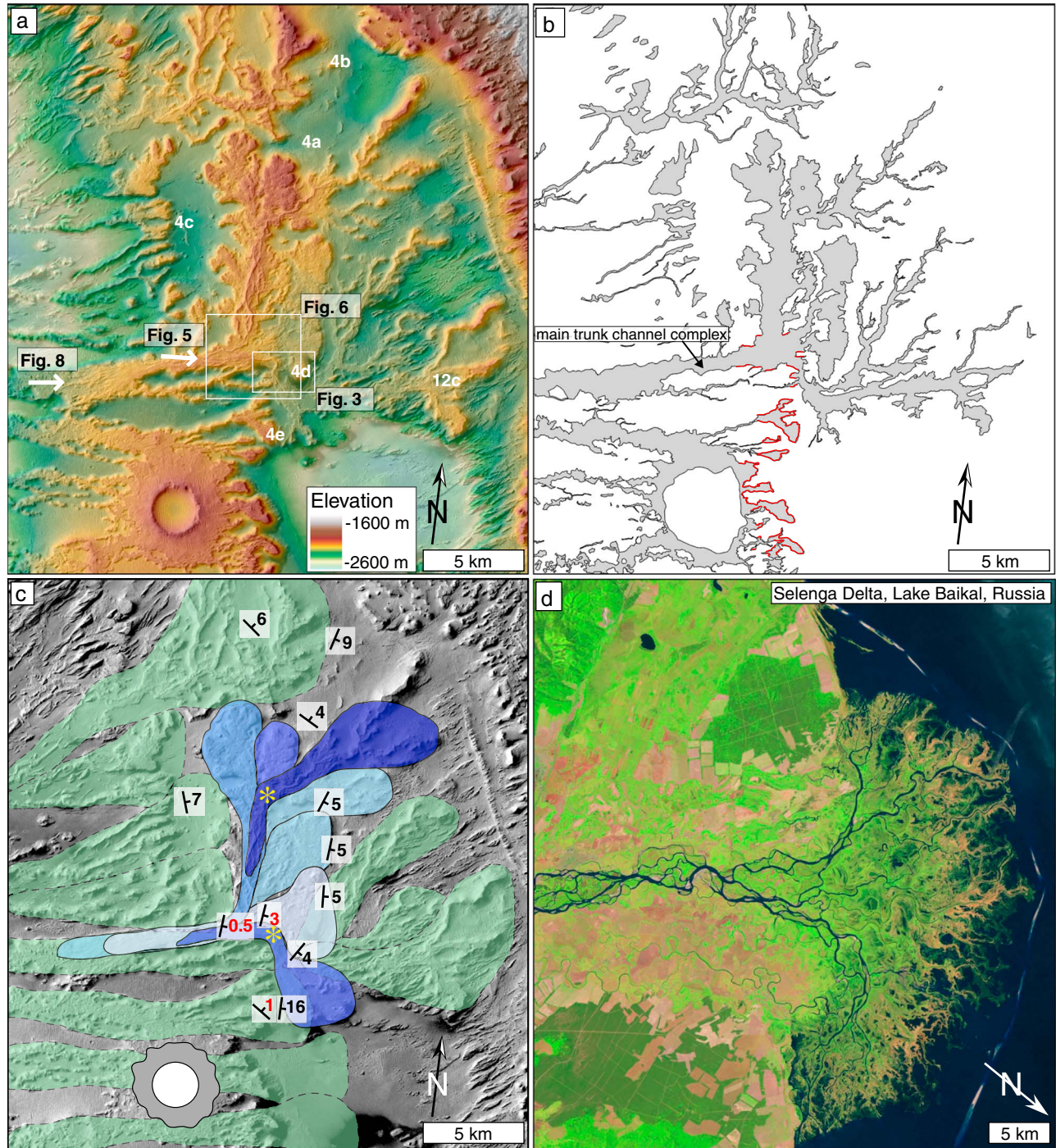
Figure 7. (a) Overview map of study area, showing CTX elevations draped over CTX imagery, and highlighting extent and viewpoints of Figures 3–8. White numbers indicate locations shown in Figures 4 and 12. (b) Map of preserved inverted channel complexes colored in gray for the region shown in Figure 7a. Red lines mark locations of caprock thickness measurements used in Figure 9. (c) Geological map of the deltaic deposits showing inferred depositional lobes (blue = well preserved; green = poorly preserved; darker shades = younger) and measurements of stratigraphic bedding plane attitudes (degrees). Red numbers indicate dip measurements inferred from caprock elevations. Stars indicate positions of the most recent lobe switches, where preserved channels show abrupt turns and elevation drops (e.g., channel in Figure 3). The Selenga river delta in Russia is shown in Figure 7d as a potential terrestrial analog displaying similar lobe and channel geometries (Table 1).
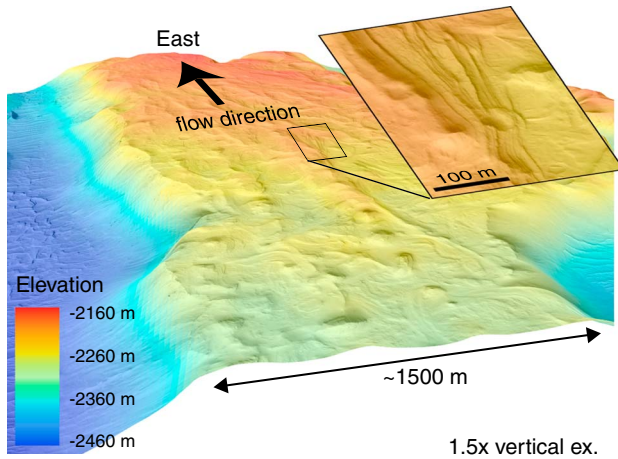
Figure 8. Perspective view to the east of main trunk channel complex showing HiRISE imagery overlain by CTX topography, highlighting the discordance between current topography and past flow direction inferred from the dip of exposed bedding planes that cut through topography (inset). Elevation of the channel complex surface increases approximately 100 m over 6 km in this view. Regional context is shown in Figure 7.

surface is locked in place, and thus the profiles of inverted channels may reflect original channel slopes, and branching channel networks can retain their planform geometry (e.g., tributary drainage networks may be preserved). Within this conceptual model, only limited superposition of inverted channels is possible—i.e., individual channels may be preserved on top of broad meander-channel belts, but crosscutting channel belts and lobes are unlikely due to the presence of confining hillslope or interfluve topography. Additionally, for the terrestrial landscape inversion examples shown in Figures 11a and 11b, there is no evidence for significant postdepositional burial, and interfluve paleotopography is preserved.

[23] Alternatively, topographic inversion can result from "deposit inversion." Here, rather than preserving a connected, coeval channel network, differential erosion of a thick sequence of fluvial and/or marine sedimentary rocks progressively exposes channels that may not have been contemporaneous (Figure 10b). While this mechanism does not preclude volcanic deposits, terrestrial examples of deposit inversion are dominated by the contrast between coarse-grained channel deposits (which due to increased porosity and permeability, tend also to be subject to more chemical cementation) versus fine-grained overbank deposits. For example, in avulsion-prone river systems, the sedimentary architecture is defined by the spatial distribution of coarser-grained channel complexes or channel bodies [e.g., *Heller and Paola*, 1996]. An important implication of this style of topographic inversion is that the modern surface topography does not typically reflect a paleogeomorphic surface due to a discordance of depositional ages. The Ebro basin in Spain shows a classic example of deposit inversion, where multiple levels of inverted meandering channel deposits are exposed in relief in the Oligocene-age Guadalope-Matarranya Formation (Figure 11c). Here, excellent outcrop control on the

sedimentary architecture of resistant sandy channel bodies aids in connecting discontinuous channel surfaces, determining paleoflow directions, and reconstructing the history of basin filling [*Mohrig et al.*, 2000; *Martinez et al.*, 2010]. A similar example occurs in the Cretaceous Cedar Mountain Formation near Green River, Utah (Figure 11d). Here, differential cementation has preserved crosscutting channel deposits that represent channels draining the Sevier mountain belt to the west [*Harris*, 1980; *Williams et al.*, 2009]. In contrast to the case of landscape inversion, the examples highlighted in Figures 11c and 11d are characterized by multiple levels of discontinuous, unconformable, crosscutting channels that reflect a wide range of flow directions typical of avulsing, depositional channels [*Slingerland and Smith*, 2004].

5.3. Application to Aeolis Dorsa

[24] For the inverted channel features at Aeolis Dorsa, the contrast between the above two topographic inversion mechanisms has not been explicitly addressed, but remains critical for interpreting flow direction and past depositional environment. *Burr et al.* [2009] and *Lefort et al.* [2012] interpreted the inverted channels in southeastern Aeolis Dorsa as representing a convergent paleodrainage network driven by landscape inversion, drawing analogy to duricrust paleolandscapes on Earth, such as the example from South Australia shown in Figure 11a [e.g., *Pain et al.*, 2007]. As shown in Figure 2, most branching features in this region converge to the west, with the notable exception of two features (35B and 35D) interpreted by *Burr et al.* [2009] as distributary fans connected to their upstream drainage network. While this interpretation is appealing in that it is generally consistent with modern topography, we propose that these features are better explained by the exhumation of a sedimentary package (i.e., deposit inversion), based on two key points.

[25] First, we observe crosscutting relationships of channels and channel complexes at a scale atypical of tributary drainage networks. In upland settings, interfluve topography (i.e., hillslopes) limits channel-belt migration, and the crosscutting of channel complexes over large scales is not
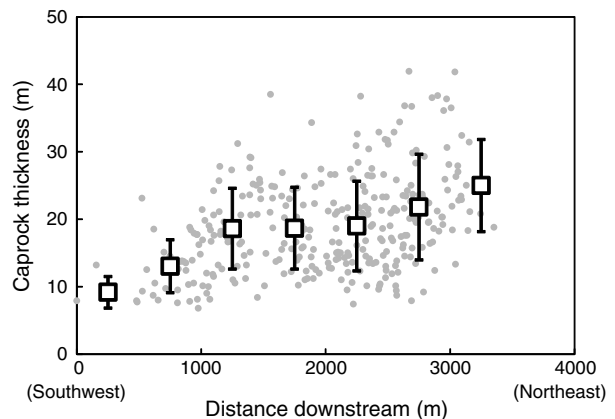

Figure 9. Plot of caprock thickness as a function of downstream distance for the full extent of the HiRISE DEM. Squares indicate 500 m binned averages ($\pm 2\sigma$). Regional context shown in Figure 7b.
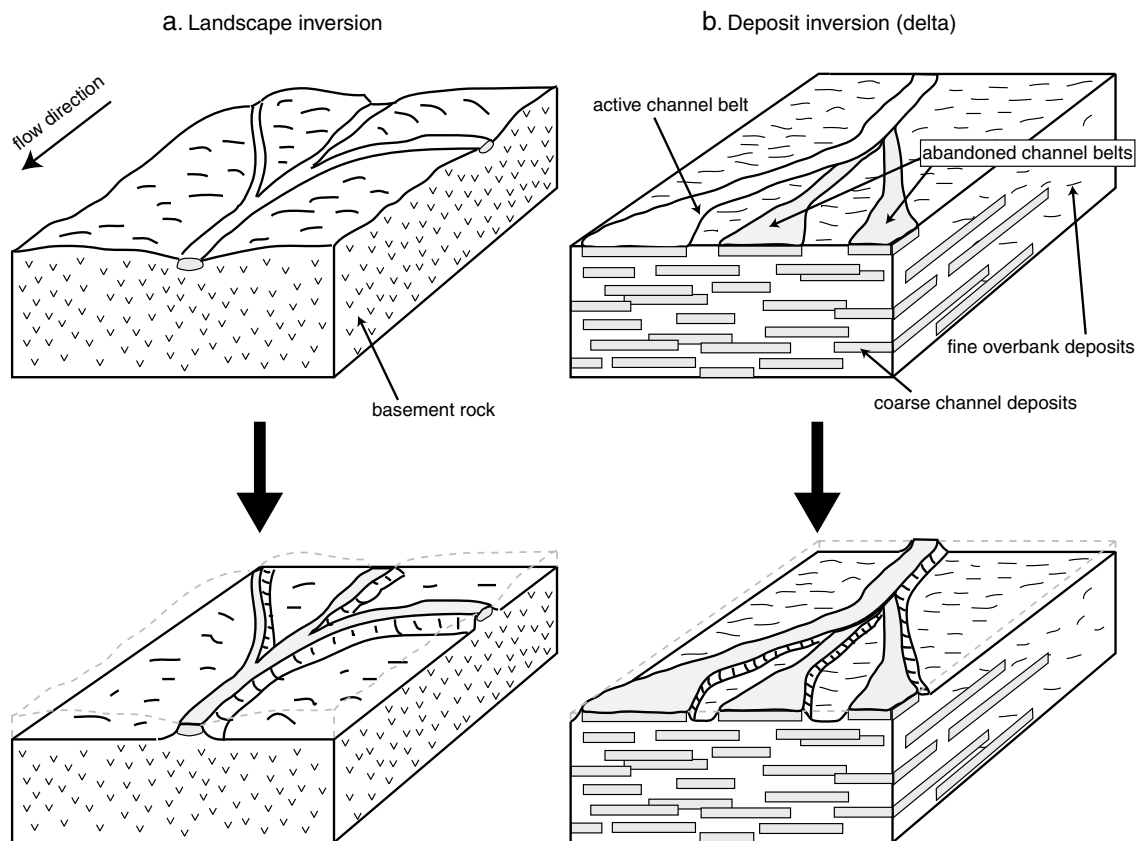
a. Landscape inversion

b. Deposit inversion (delta)

Figure 10. Schematic showing different inversion mechanisms and scenarios. In the case of (a) landscape inversion, a tributary network of incising channels is mantled with material more resistant than the surrounding interfluves and is preserved as a tributary network of coeval inverted channels. For the case of (b) deposit inversion, an aggrading, in this case avulsing, channel network builds a sedimentary deposit consisting of coarse channel fill and fine overbank material, which is differentially eroded to reveal channel deposits with discordant ages.

expected. However, in depositional settings, even in the absence of confining hillslopes, channels tend to cluster into channel belts, and the crosscutting of both individual channels and channel-belt complexes is common and defines the stratigraphic architecture of such deposits [*Heller and Paola*, 1996]. If the inverted channels in Figure 2 represent a coeval network, the only areas expected to have such crosscutting channels would be the two fans mapped at 35B and 35D. However, we find multiple areas in east-branching networks with crosscutting channels (Figures 12b–12d), and for our mapped study area, we show evidence for crosscutting of channel complexes (Figure 7c). These observations are difficult to reconcile within a tributary drainage network interpretation, but are characteristic of depositional systems dominated by avulsing channels and lobes (Figure 12a). We hypothesize that the inverted channels exposed in Figure 2 represent multiple stratigraphic levels, and thus varying geomorphic surfaces. Our interpretation differs from that presented by *Burr et al.* [2009] to explain "multilevel" channels, in that we observe the abundant crosscutting of separate channel-belt complexes that were not necessarily confined by interfluve topography, in addition to the local crosscutting of individual channels. Furthermore, at a regional scale, there appears to be a systematic change in the nature of the inverted channels with stratigraphic level,

with wispy channel deposits overlying more pronounced narrow and flat-topped deposits that show higher sinuosity meander bends [*Burr et al.*, 2009], suggesting a temporal change in paleoenvironment over geologic timescales.

[26] The second point of support for deposit inversion is based on arguments in our study area for flow to the east, counter to the modern regional topographic slope. We interpret flow to the east based on the presence of channels dropping in elevation to the east (e.g., Figure 3), the prevalence of bedding planes dipping to the east (Figure 7c), and the eastward thickening of the caprock unit (Figure 9). As noted above, in two locations (stars, Figure 7c) we observe well-preserved paleochannels that change direction and drop ~100 m to the east, a scale larger than the measured thickness of channel bodies—a feature that cannot be explained by differential surface erosion. We find no evidence for similar features dipping to the west. Additionally, our measured bedding attitudes from multiple stratigraphic levels dip generally to the east, and the dip magnitudes steepen to the east (Figure 7c) consistent with depositional clinoforms with paleoflow to the east. Even if the absolute dip magnitudes have been distorted due to regional deformation, this would not affect the relative dips of stratigraphic sequences in contact with one another that show steepening to the east over kilometer scales or less. If the inverted channel network
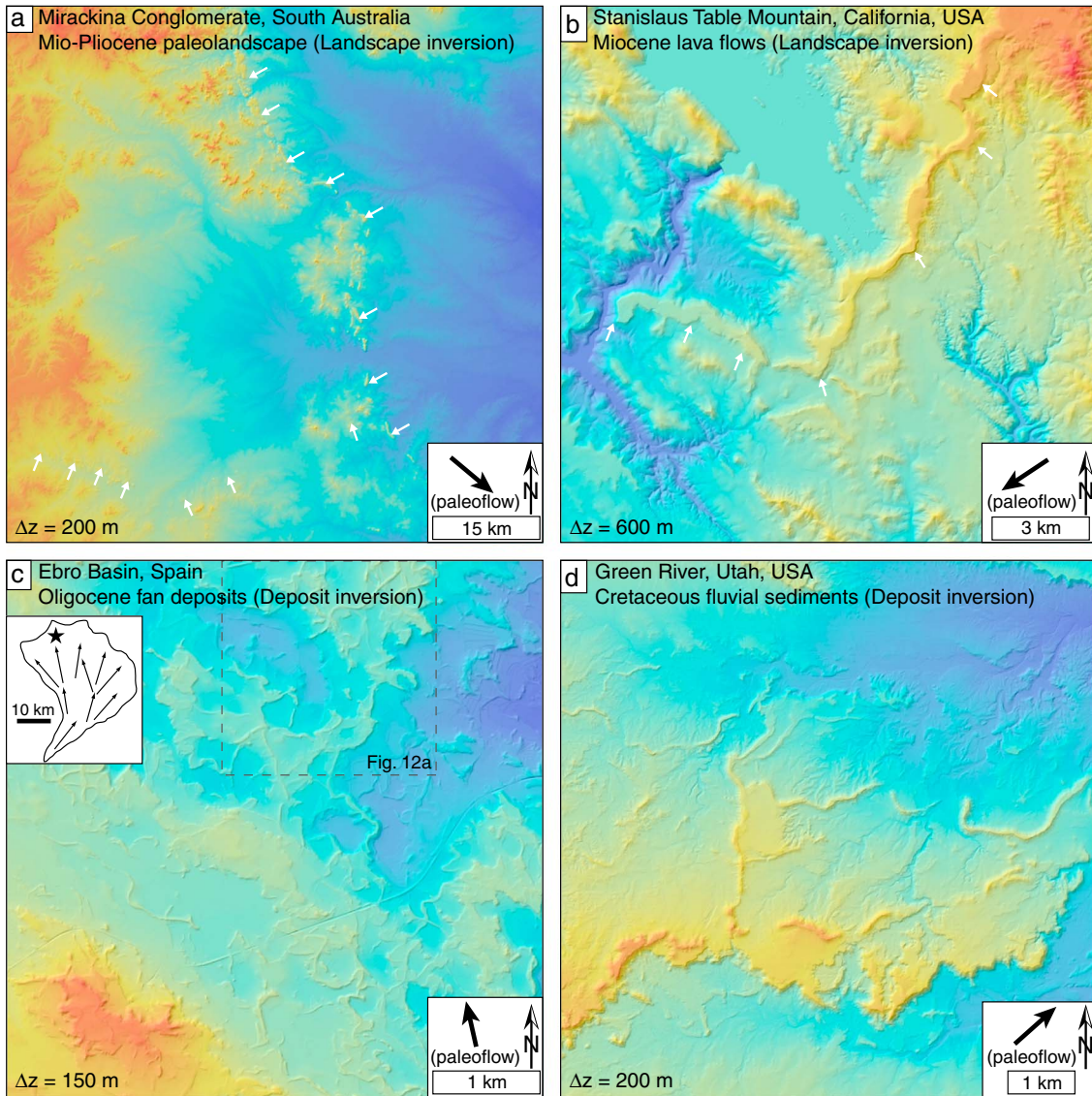
Figure 11. Elevation and hillshade maps of terrestrial inverted channel analogs, highlighting examples of (a, b) landscape inversion and (c, d) deposit inversion. For each panel, Δz indicates the difference in meters between the highest (red) and lowest (blue) elevations. DEM resolution is 30 m, 10 m, and 5 m. Black arrows indicate general paleoflow direction based on outcrop observations [*Harris*, 1980; *Rhodes*, 1980; *Pain and Ollier*, 1995; *Williams et al.*, 2009; *Martinez et al.*, 2010]. White arrows in Figures 11a and 11b define channel deposits for landscape inversion cases. Inset map in Figure 11c shows location of panel c within larger fan deposit [*Martinez et al.*, 2010], and dashed box indicates extent of Figure 12a. Note the difference in hillslope preservation between landscape inversion and deposit inversion examples.

shown in Figure 7 was formed by landscape inversion of a convergent tributary network, we would expect bedding planes to dip to west, with headwater (eastern) channel deposits dipping strongly to the west. Finally, we observe an eastward thickening of the caprock unit (Figure 9) that we interpret as representing greater deposition to the east, a pattern typical of distributary fans where deposition increases downstream. If interpreted as a convergent network flowing to the west, we would instead expect an eastward thinning of channel deposits. Overall, these observations are consistent with geometries found in distributary channel networks and fans that are typical of depositional systems, and inconsistent with a coeval tributary fluvial system.

[27] Thus, a broad range of observations throughout the region supports the idea that the observed sinuous ridges comprise channel elements being differentially eroded from a sedimentary succession that need not be connected to a modern upland source basin depending on deposit age and preservation [e.g., *Ansan et al.*, 2011]. Consequently, we interpret these sinuous ridges as deposits from branching and anastomosing channels within finer-grained sediments—a common mode of stratigraphic architecture in clastic sedimentary rocks on Earth [e.g., *Heller and Paola*, 1996; *Mohrig et al.*, 2000; *Gibling*, 2006]. Much is known about the stratigraphic architecture of channel bodies within fluvial, deltaic, and marine deposits on Earth, including details of the
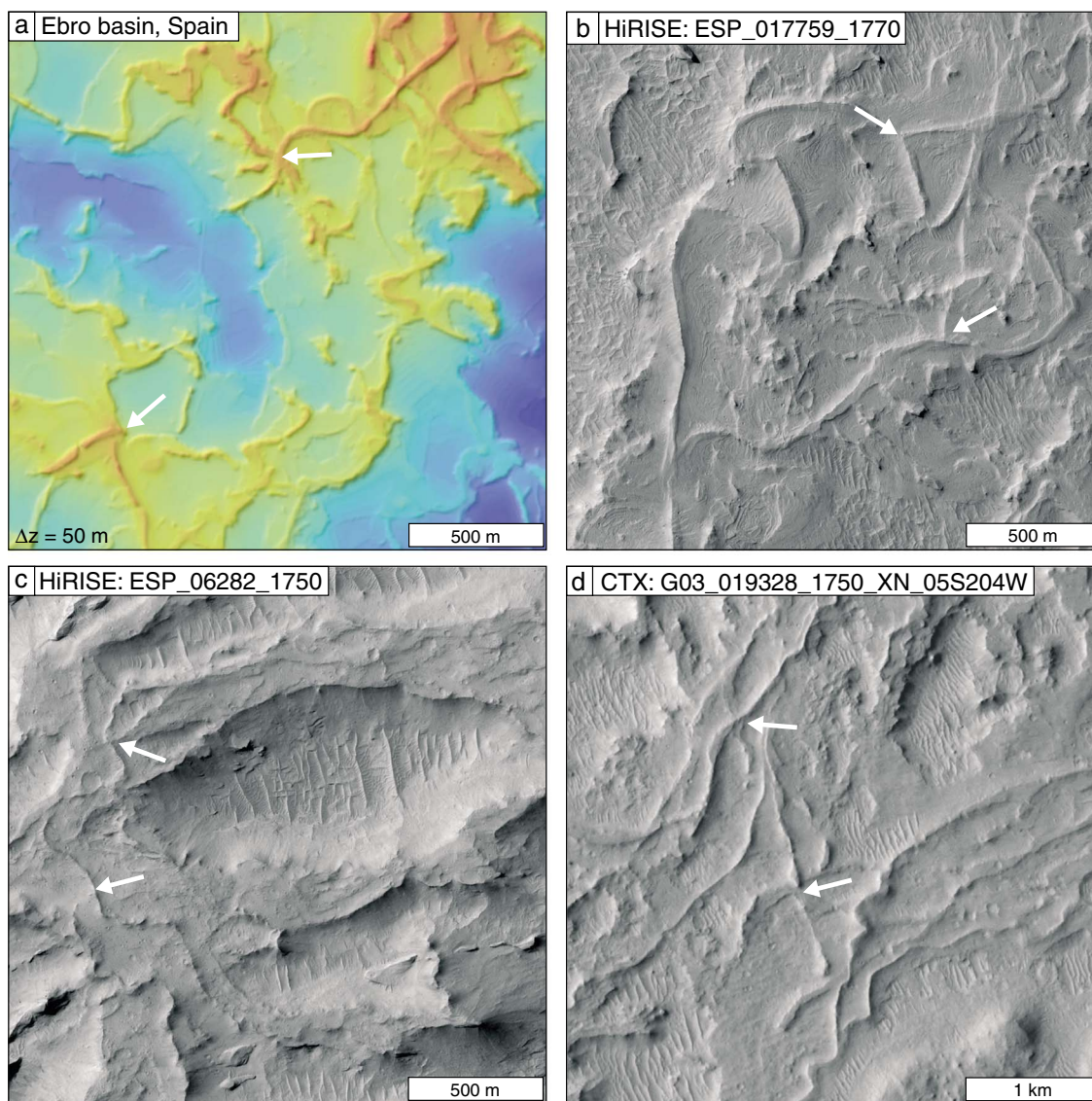
Figure 12. Comparison of crosscutting channel features between (a) Ebro Basin deposits and (b–d) examples from CTX and HiRISE imagery at Aeolis Dorsa. North is up in all panels. Regional context for Figures 12c and 12d shown in Figure 2.

processes of sediment transport that create them. In this study, we bring this terrestrial insight to bear on the deposits of Aeolis Dorsa with commensurate interpretations based on an expectation of uniformitarian physical processes.

5.4. Determining Depositional Environment

[28] There are three possible broad deposit types that need to be considered and are differentiated depending on whether the depositional environment was subaerial (alluvial fan hypothesis), subaqueous (submarine fan hypothesis), or coastal (delta hypothesis). As shown in Figure 7c, the planform geometry of the inverted channels suggests a common avulsion node for all depositional lobes associated with a main trunk channel complex (blue polygons in Figure 7c). This lobe system is characterized by sharp changes in flow direction (e.g., lobe switching), evidence for deposition tending towards areas of greater accommodation (stars in Figure 7c), and a thick deposit comprising the trunk channel complex,

indicating net aggradation for at least 10 km upstream of the observed avulsion node (Figure 8). To the north and south, a series of similarly sized channel complexes lie at approximately the same stratigraphic and along-stream location as the main trunk system (Figures 7a and 7b). While the associated distributary lobate deposits are not as well preserved for these parallel systems (green polygons, Figure 7c), we interpret these features as reflecting similar processes as the main trunk system. We can use the above observations of lobe geometries to test the subaerial fan hypothesis. Because the deposition of subaerial fans is fundamentally driven by a change in topographic confinement (such as a canyon-bound river exiting a mountain range, or a tributary entering a large valley), we would expect that (1) the node of avulsion is tied to a change in confinement, and (2) upstream of this point, the channel system tends to be net erosional [*Blair and McPherson*, 2009]. As we observe areas of high modern topography in this region to correspond to

Table 1. Flow Calculations

Parameter	Aeolis (Sand)[a]	Aeolis (Gravel)[a]	Selenga Delta, Russia[b]
Avulsion length scale (km)	10	10	30
Meander belt width (m)	1500	1500	3000
Channel width (m)	50–100	50–100	300
Channel depth (m)	5–10	5–10	9[b]
Slope (m/m)	0.0005–0.001	0.0005–0.001	0.0003
Bed load grain size (mm)	0.6–2.3	19–77	–
Water discharge (m^3/s)	740–5200	400–2900	897
Total water volume (km^3)	7×10^4–2×10^5	7×10^5–2×10^6	–
Sediment flux (m^3/yr)	1×10^6–2×10^7	9×10^4–1×10^6	1×10^6
Min. formation time (years)	400–7000	7300–120,000	–

[a]Sediment flux and formation time results do not incorporate intermittency factor.
[b]Channel depth is estimated using $H = L/S$. Water discharge corresponds to mean annual discharge of Selenga River just upstream of delta (1941–2008). Sediment flux corresponds to long-term suspended sediment load measurements at same location [*Potemkina*, 2011].

channel deposits, and interpret the region on the whole as a thick sedimentary deposit (Figures 1 and 2), the absence of past confining bedrock topography, such as a canyon-bound river channel, is incompatible with an alluvial fan; the presence of thick and extensive deposits within the trunk channel complex suggests a net aggradational, rather than erosional feeder channel. Furthermore, the high stratigraphic dips observed in the depositional lobes contrast with the lower gradient feeder channel—a stratigraphic architecture that is not consistent with a subaerial fan. Consequently, we reject the subaerial fan hypothesis for the genesis of these deposits.

[29] In contrast to alluvial fans, submarine fans typically have longer sediment travel distances, lower slopes, and self-leveed channels [*Covault*, 2011]. While the driver for sedimentation in both environments is similar (i.e., change in confinement or regional slope break), differences in flow dynamics between turbidity currents and rivers translate into differences in both the planform geometry and the sedimentary architecture of deposits. Specifically, submarine fan deposits tend to form discrete, tabular lobes with slopes less than a few degrees and width-depth ratios of 100:1 or greater [*Prelat et al.*, 2010]. Determining the thickness of the lobes in Figure 7 is difficult due to debris-covered side slopes, but using the exposed caprock thickness as a minimum estimate gives a value of 10–30 m. The width of the lobes is on the order of 5 km, giving a maximum width-depth ratio of ~500:1, which is consistent with a compilation of submarine fan lobe measurements [*Prelat et al.*, 2010]. Submarine fan deposits have also been described on Mars; *Metz et al.* [2009] used the elongate planform geometry of fan lobes and low bedding dips (<1°) of deposits exposed in Valles Marineris to argue for a subaqueous fan origin. However, while the steep dips (up to 16°) observed in our study area (Figure 7) are not necessarily incompatible with a submarine-fan environment [e.g., *Prelat et al.*, 2010], turbidity currents are unlikely to produce the observed sharp deviation

angles of the lobes and channel elements in the absence of significant topographic obstructions [*Kneller and Buckee*, 2000; *Lamb et al.*, 2004]. Furthermore, the presence of abrupt changes in channel direction at approximately the same elevation (white circles, Figure 6) implies that avulsions were controlled by a common base level, such as sea level.

[30] Deltaic deposits are driven by backwater effects that commonly fix the node of avulsion or lobe switching to a characteristic distance upstream of the shoreline that depends on river-flow depth and water-surface slope [*Slingerland and Smith*, 2004; *Jerolmack*, 2009; *Chatanantavet et al.*, 2012]. As noted above, our mapping indicates that the channel branching patterns and lobe switching are largely tied to a single point and are not associated with any observable change in confinement (Figure 7). Furthermore, two of the most recently active (and well-preserved) inverted paleochannels visible on the exhumed deposit take sharp turns and locally drop ~100 m in elevation, indicating a switch in depocenter towards lower topography (stars in Figure 7c). These switches are qualitatively consistent with observations of channel avulsions in deltas on Earth (Figure 7d). Perhaps, the most distinguishing feature of terrestrial deltaic deposits is the pattern of regional slope breaks in depositional surfaces that delineate gently dipping topsets, steeply dipping foresets, and gently dipping bottomsets [*Gilbert*, 1885]. Critically, we observe evidence for steeply dipping beds (4–16°) that we interpret as foresets of clinoforms near the toes of mapped depositional lobes (Figure 7) and use the nearly flat (<1°) attitude of the 10–30 m caprock elevating the trunk feeder channel complex as evidence for a gently dipping topset beds. With the current exposure, we lack evidence for bottomset deposits. It is possible that they remain covered by the younger units of the MFF seen covering this clastic wedge to the east and north, but such features may also be difficult to preserve due to downstream fining and a consequent decline of resistant channel deposits to sustain inverted topography. Figure 7 also highlights steeply dipping bedding planes elsewhere in the deposit and not associated with the most recently active depositional lobes. We interpret these prominent dipping layers as older foresets of clinoforms based on their lower elevation and spatial relation to the paleoshoreline implied by lobe switching. This, along with the pattern of downstream thickening observed in the caprock unit (Figure 9), highlights a prograding delta front as the most likely depositional environment.

6. Paleodelta Water and Sediment Discharge Analysis

[31] Reconstructing paleoflow conditions within the channels and deposit formation timescales requires estimating hydraulic geometry parameters (i.e., channel depth, width, and slope) from remote sensing data. *Mohrig et al.* [2000] demonstrated that channel body thickness can be used as an approximate scale for channel depth given that channels tend to avulse (in a probabilistic sense) when bed aggradation exceeds approximately one channel depth. We used measurements of the thickness of the caprock from the trunk feeder channel complex, which ranges from 10 to 30 m, as a measure of channel body thickness and therefore channel

depth (Figure 9). We favor the upstream, lower end of this range, as the inverted morphologies here suggest that the channel was likely single threaded, and because this number is likely a maximum if the caprock represents multiple amalgamated channel bodies. However, this depth will be only a rough approximation and sensitive to postdepositional erosion. In addition, we can estimate depth from fluvial width-to-depth ratios or from compilations of meander-belt channel body width-to-depth ratios, which for deposits on Earth tend to fall within a narrow range [*Gibling*, 2006; *Parker et al.*, 2007]. For our area, preserved individual paleochannels are 50–100 m wide and correspond to bankfull flow depths of 1–10 m assuming width-to-depth ratios of 10–60 [*Parker et al.*, 2007]. If we instead use empirical relationships for meander-channel-belt sand bodies, the width of our channel complexes (~1500 m) corresponds to flow depths of ~5 m [*Bridge and Mackey*, 1993]. It is encouraging that the three independent estimates of paleoflow depth are broadly consistent, and we use the range from 5 to 10 m for our calculations.

[32] While it is possible to infer channel width and flow depth directly, measuring the slope of the feeder channel complex accurately is challenging. Identifying temporally correlative channel features and vertical errors over short distances (~1 km) makes it difficult to accurately measure slopes of substantially less than 1°. Instead, we used an empirical scaling law for deltas to determine slope. The avulsion length scale L of terrestrial deltas scales with the channel bed slope S and characteristic flow depth H as $L \sim H/S$ and represents the length scale over which backwater effects influence channel processes [*Jerolmack*, 2009; *Chatanantavet et al.*, 2012; *Lamb et al.*, 2012]. Thus, we can use estimates of channel flow depth and measurements of depositional lobe size to calculate the channel-bed slope. To determine the avulsion length scale, we used the distance from the avulsion node on the trunk channel complex to the end of the best preserved depositional lobe to obtain a value of 10 km. We used the relationship $S = H/L$ to calculate a slope gradient ranging from 5×10^{-4} to 1×10^{-3} (0.03° to 0.06°).

[33] The calculated slopes can be used to estimate grain size under the assumption that the formative Shields stress ($\tau_{*b} = HS/RD$, where R is submerged specific particle density, and D is grain diameter) associated with bankfull conditions is constant for a given bed sediment size. For example, in gravel-bed rivers, the bankfull Shields stress is typically 1.2 times the critical value of the Shields stress at incipient sediment motion ($\tau_{*c} = 0.045$), i.e., $\tau_{*b} = 1.2\tau_{*c} = 0.054$ [*Parker et al.*, 2007]. Alternatively, values for sand-bed rivers indicate $\tau_{*b} = 1.8$ [*Parker*, 2008]. Using the above estimates for depth and slope, and a value of 2.4 for R (assuming sediment of basaltic composition in water), the resulting grain diameters range from 19 to 77 mm and 0.6 to 2.3 mm for the gravel-bed and sand-bed assumptions, respectively. Grain-size estimates based on the sand-bed and gravel-bed assumptions are both internally consistent, and thus we cannot distinguish between the two cases. We proceed with a reconstruction for both the sand- and gravel-bed cases.

[34] To calculate water discharge for the formative flows described above, we combined channel width and depth measurements with flow velocity, estimated using a flow resistance equation. Assuming a gravel bed, we used a Manning-Strickler relation to relate cross-sectional average velocity, U, to grain size and flow depth according to $U/u_* = 8.1 (H/k_s)^{1/6}$, where u^* is the shear velocity and k_s is a roughness length scale equal to $3D$ [*Parker*, 1991]. For sand-bed rivers, form drag due to bed forms necessitates the use of a friction value incorporating the influence of dunes ($U/u^* = 10$) [e.g., *Fedele and Garcia*, 2001]. We combined these relationships with an equation for conservation of mass ($Q_w = UWH$) to calculate a formative water discharge, Q_w, ranging from 400 to 5200 m³/s depending on bed material (Table 1).

[35] We used standard sediment transport equations for sand-bed [*Engelund and Hansen*, 1967] and gravel-bed [*Meyer-Peter and Müller*, 1948] rivers, coupled with empirical relationships for typical sediment transport stage to estimate instantaneous water and sediment fluxes. Under the assumption that $\tau_{*b} = 1.2\tau_{*c}$ for formative flows in gravel-bed rivers, and $\tau_{*b} = 1.8$ for sand-bed rivers, we calculated a sediment flux ranging from 9×10^4 to 2×10^7 m³/yr assuming continuous flow at bankfull discharge (Table 1). Using a mean thickness of 100 m for the depositional lobes associated with the main trunk channel complex (blue polygons, Figure 7), we estimated a total sediment volume of ~10 km³, which implies a minimum formation timescale (i.e., continuous flows) of 400 years for a sand-bed case and 740 years for a gravel-bed case. The total water volume that is needed to form the observed deposits is of order 10^5–10^6 km³. Rivers on Earth only transport sediment intermittently (i.e., during floods), and if we incorporate a typical intermittency factor [sensu *Paola et al.*, 1992] for rainfall or snowmelt events of 0.01, our estimates of formation timescale increase accordingly to 40,000 and 74,000 years. For comparison, we also show discharge and sediment flux data for the Selenga River delta feeding Lake Baikal, Russia (Figure 7d, Table 1). The Selenga delta has a strikingly similar planform network, similar channel dimensions, and consequently similar estimates of water and sediment flux to our delta.

7. Implications for a Hemispheric Ocean

[36] Our focused study area (Figure 7a) contains one of several features with similar morphology observed within the broader region shown in Figure 2, which itself makes up a small part of the greater Aeolis Dorsa region (dashed outline, Figure 1). While additional stratigraphic analysis is needed, the similarity between inverted channel deposits in our area and the rest of Aeolis Dorsa as revealed by CTX and HiRISE image analysis suggests a similar origin [e.g., *Burr et al.*, 2009]. Namely, it is unlikely that these features are representative of a coeval geomorphic surface, and instead indicate an extensive fluvial or marine sedimentary deposit spanning approximately 10^5 km². Our observations and analysis of the branching network of inverted channels shown in Figure 7 reveal a long-lived deltaic depositional environment—an interpretation that has important implications for a standing body of water during the time of deposition. The absence of clear inverted fluvial features to the east and west of Aeolis Dorsa [*Burr et al.*, 2009] may reflect either the limited extent of this sea, or simply a limited exposure of these deposits through an erosional window of the upper units

in the MFF. Based solely on current topography, standing water in the region of Aeolis Dorsa would imply an ocean covering a substantial portion of the northern lowlands. However, much of the area north of Aeolis Dorsa has been resurfaced by Amazonian volcanism associated with Elysium Mons and Cerberus Fossae [*Tanaka et al.*, 2005]. The present lack of evidence for similar deposits elsewhere along the dichotomy boundary may be due to local preservation and/or exposure of the deposits at Aeolis Dorsa following emplacement of the MFF. Finally, any evidence for potential sources of sediment and water south of the dichotomy boundary has likely been eroded, in contrast to the canyon-fed fans and deltas at Eberswalde, Jezero, and Melas, where feeder valley networks connected to the deposits are preserved.

[37] While the absolute age constraints on the deposits at Aeolis Dorsa remain loose, the absence of incised feeding valleys (like the large, well-preserved valley networks preserved elsewhere along the dichotomy [e.g., *Irwin et al.*, 2005]) leads us to speculate that these deposits are the result of an earlier period of fluvial activity than that observed at Eberswalde, Jezero, and Melas, and that the catchments have since been eroded. Most of the putative deltas in the compilation of *Di Achille and Hynek* [2010] are connected to upstream valleys and represent localized deposits that may be related to late-stage fluvial activity (i.e., Hesperian or younger). In contrast, the large spatial extent of the deposits at Aeolis Dorsa and observations of multiple, superposed branching distributary channel networks suggest that it is unlikely for potential source watersheds to be preserved, much like it is for ancient sedimentary deposits on Earth. The layered deposits at Terby crater in Hellas Basin interpreted as deltaic by *Ansan et al.* [2011] provide an opportunity for comparison that may help estimate the timing of the deposits at Aeolis Dorsa. As is the case for the sedimentary deposits in Aeolis Dorsa, no upland source of water and sediment is preserved at Terby. The deposits in Terby crater, which are interpreted to be Noachian in age based on crater counting statistics, show evidence of later reworking in the form of incised valleys and fans [*Ansan et al.*, 2011]. We speculate that the deposits at Aeolis Dorsa are more likely to be coeval with deposition at Terby crater than with late-stage fans and deltas such as Eberswalde [*Mangold et al.*, 2012] and may capture an early wetter interval in Mars history with active sedimentary basins and large bodies of water in both Hellas and the northern lowlands of Mars. Further investigation of similar deposits at Aeolis Dorsa and elsewhere using increasingly available high-resolution orbital stereo-imagery will provide valuable insight into the early water budget of these regions.

8. Conclusions

[38] We interpret the branching network of sinuous ridges in Figure 7 as channel elements within deposits of an ancient sedimentary delta based on three primary observations. First, evidence for stacked and crosscutting channels and channel complexes, well-preserved paleochannels that drop in elevation to the east, east-dipping bedding planes, and eastward thickening of a prominent caprock layer indicate that this feature is an exhumed deposit built by a distributary network of channels flowing to the east, rather than a preserved convergent drainage network flowing to the west. Second, the lack

of evidence for a change in topographic confinement and the presence of aggradational trunk feeder channels are incompatible with formation by a tributary drainage network or alluvial fan, and the branching patterns of the channel lobes originate from a single node and often show sharp deviations in flow direction, features atypical of submarine-fan processes but characteristic of fluvio-deltaic systems. Additionally, the presence of channel lobe switches occurring at similar elevations suggests a base-level control on the avulsion node such as sea level. Third, measurements of stratigraphic bedding plane attitudes are consistent with lobe geometries and show a transition from low-angle topsets to steeply dipping foreset clinoforms typical of terrestrial deltas.

[39] For our proposed delta, we determined channel geometries using scaling relationships and arguments developed for terrestrial fluvial and deltaic systems. We measured channel width based on the width of preserved individual paleochannels; we inferred flow depth based on width-to-depth ratios for both channels and channel belts, as well as from the measured caprock thickness; and we calculated slope based on the ratio of flow depth to the backwater length scale determined from depositional lobe size. Based on sediment transport calculations, we determined a minimum delta formation timescale of 400 years (with no intermittency), requiring 10^5–10^6 km^3 of water for this portion of the deposit. Both the time and amounts of water involved in the deposition of the entire sedimentary succession observed at Aeolis Dorsa are likely much greater.

[40] Our analysis indicates that the inverted channel features found throughout Aeolis Dorsa comprise an extensive clastic sedimentary sequence onlapping the crustal dichotomy. The location of our delta and other similar features within Aeolis Dorsa implies a large standing body of water spanning at least 10^5 km^2 and potentially far larger based on a complete lack of confining topography. The coincidence of these features with the hypothesized location of a hemispheric ocean in the northern plains of Mars makes the channel-rich deposits at Aeolis Dorsa a key area for future stratigraphic investigation.

References

Aharonson, O., M. T. Zuber, and D. H. Rothman (2001), Statistics of Mars' topography from the Mars Orbiter Laser Altimeter: Slopes, correlations, and physical Models, *J. Geophys. Res.*, *106*(E10), 23,723–23,735, doi:10.1029/2000je001403.

Ansan, V., et al. (2011), Stratigraphy, mineralogy, and origin of layered deposits inside Terby crater, Mars, *Icarus*, *211*(1), 273–304, doi:10.1016/j.icarus.2010.09.011.

Baker, V. R., and D. J. Milton (1974), Erosion by catastrophic floods on Mars and Earth, *Icarus*, *23*(1), 27–41, doi:10.1016/0019-1035(74)90101-8.

Baker, V. R., R. G. Strom, V. C. Gulick, J. S. Kargel, G. Komatsu, and V. S. Kale (1991), Ancient oceans, ice sheets and the hydrological cycle on Mars, *Nature*, *352*(6336), 589–594, doi:10.1038/352589a0.

Bhattacharya, J. P., T. H. D. Payenberg, S. C. Lang, and M. Bourke (2005), Dynamic river channels suggest a long-lived Noachian crater lake on Mars, *Geophys. Res. Lett.*, *32*, L10201, doi:10.1029/2005gl022747.

Blair, T. C., and J. G. McPherson (2009), Processes and forms of alluvial fans, in *Geomorphology of Desert Environments*, edited by A. J. Parsons and A. D. Abrahams, pp. 413-467, Springer, New York.

Bridge, J. S., and S. D. Mackey (1993), A theoretical study of fluvial sandstone body dimensions, in *The Geologic Modelling of Hydrocarbon Reservoirs*, edited by S. S. Flint, and I. D. Bryant, Spec. Publ. Int. Assoc. Sedimentol., *15*, 213–236.

Buhler, P. B., C. I. Fassett, J. W. Head, and M. P. Lamb (2011), Evidence for paleolakes in Erythraea Fossa, Mars: Implications for an ancient hydrological cycle, *Icarus*, *213*(1), 104–115, doi:10.1016/j.icarus.2011.03.004.

Burr, D. M., M. T. Enga, R. M. E. Williams, J. R. Zimbelman, A. D. Howard, and T. A. Brennand (2009), Pervasive aqueous paleoflow features in the Aeolis/Zephyria Plana region, Mars, *Icarus*, *200*(1), 52–76, doi:10.1016/j.icarus.2008.10.014.

Burr, D. M., R. M. E. Williams, K. D. Wendell, M. Chojnacki, and J. P. Emery (2010), Inverted fluvial features in the Aeolis/Zephyria Plana region, Mars: Formation mechanism and initial paleodischarge estimates, *J. Geophys. Res.*, *115*, E07011, doi:10.1029/2009je003496.

Cabrol, N. A., and E. A. Grin (1999), Distribution, classification, and ages of martian impact crater lakes, *Icarus*, *142*(1), 160–172, doi:10.1006/icar.1999.6191.

Carr, M. H. (1996), *Water on Mars*, Oxford Univ. Press, New York.

Carter, L. M., et al. (2009), Shallow radar (SHARAD) sounding observations of the Medusae Fossae Formation, Mars, *Icarus*, *199*(2), 295–302, doi:10.1016/j.icarus.2008.10.007.

Chatanantavet, P., M. P. Lamb, and J. A. Nittrouer (2012), Backwater controls of avulsion location on deltas, *Geophys. Res. Lett.*, *39*, L01402, doi:10.1029/2011gl050197.

Clifford, S. M., and T. J. Parker (2001), The evolution of the Martian hydrosphere: Implications for the fate of a primordial ocean and the current state of the northern plains, *Icarus*, *154*(1), 40–79, doi:10.1006/icar.2001.6671.

Covault, J. A. (2011), Submarine fans and canyon-channel systems: A review of processes, products, and models, *Nat. Educ. Knowl.*, *3*(10), 4.

Craddock, R. A., and A. D. Howard (2002), The case for rainfall on a warm, wet early Mars, *J. Geophys. Res.*, *107*(E11), 5111, doi:10.1029/2001je001505.

Di Achille, G., and B. M. Hynek (2010), Ancient ocean on Mars supported by global distribution of deltas and valleys, *Nat. Geosci.*, *3*(7), 459–463, doi:10.1038/ngeo891.

Ehlmann, B. L., J. F. Mustard, C. I. Fassett, S. C. Schon, J. W. Head, D. J. D. Marais, J. A. Grant, and S. L. Murchie (2008), Clay minerals in delta deposits and organic preservation potential on Mars, *Nat. Geosci.*, *1*(6), 355–358, doi:10.1038/ngeo207.

Engelund, F., and E. Hansen (1967), A monograph on sediment transport in alluvial channels, Teknik Forlag, Copenhagen.

Fairen, A. G., J. M. Dohm, V. R. Baker, M. A. de Pablo, J. Ruiz, J. C. Ferris, and R. C. Anderson (2003), Episodic flood inundations of the northern plains of Mars, *Icarus*, *165*(1), 53–67, doi:10.1016/s0019-1035(03)00144-1.

Fassett, C. I., and J. W. Head (2005), Fluvial sedimentary deposits on Mars: Ancient deltas in a crater lake in the Nili Fossae region, *Geophys. Res. Lett.*, *32*, L14201, doi:10.1029/2005gl023456.

Fassett, C. I., and J. W. IIIHead (2008), Valley network-fed, open-basin lakes on Mars: Distribution and implications for Noachian surface and subsurface hydrology, *Icarus*, *198*(1), 37–56, doi:10.1016/j.icarus.2008.06.016.

Fedele, J. J., and M. H. Garcia (2001), Hydraulic roughness in alluvial streams: a boundary layer approach, in *Riverine, Coastal, and Estuarine Morphodynamics*, edited by G. Seminara, and P. Blondeaux, pp. 37–60, Springer-Verlag, Berlin.

Fishbaugh, K. E., S. Byrne, K. E. Herkenhoff, R. L. Kirk, C. Fortezzo, P. S. Russell, and A. McEwen (2010), Evaluating the meaning of "layer" in the martian north polar layered deposits and the impact on the climate connection, *Icarus*, *205*(1), 269–282, doi:10.1016/j.icarus.2009.04.011.

Ghatan, G. J., and J. R. Zimbelman (2006), Paucity of candidate coastal constructional landforms along proposed shorelines on Mars: Implications for a northern lowlands-filling ocean, *Icarus*, *185*(1), 171–196, doi:10.1016/j.icarus.2006.06.007.

Gibling, M. R. (2006), Width and thickness of fluvial channel bodies and valley fills in the geological record: A literature compilation and classification, *J. Sediment. Res.*, *76*(5-6), 731–770, doi:10.2110/jsr.2006.060.

Gilbert, G. K. (1885), The topographic features of lake shores, *U.S. Geol. Surv., Fifth Annual Report*, pp. 69–123, Washington, D. C.

Goudge, T. A., J. W. Head, J. F. Mustard, and C. I. Fassett (2012), An analysis of open-basin lake deposits on Mars: Evidence for the nature of associated lacustrine deposits and post-lacustrine modification processes, *Icarus*, *219*(1), 211–229, doi:10.1016/j.icarus.2012.02.027.

Greeley, R., and J. E. Guest (1987), Geologic map of the eastern equatorial region of Mars *U.S. Geol. Surv. Misc. Invest.*, Map I-1802-B, 1:15,000,000.

Grotzinger, J. P., et al. (2005), Stratigraphy and sedimentology of a dry to wet eolian depositional system, Burns formation, Meridiani Planum, Mars, *Earth Planet. Sci. Lett.*, *240*(1), 11–72, doi:10.1016/j.epsl.2005.09.039.

Haberle, R. M. (1998), Early Mars climate models, *J. Geophys. Res.*, *103*(E12), 28,467–28,479, doi:10.1029/98je01396.

Harris, D. R. (1980), Exhumed paleochannels in the Lower Cretaceous Cedar Mountain Formation near Green River, Utah, *Brigham Young Univ. Geol. Stud.*, *27*(1), 51–66.

Head, J. W., H. Hiesinger, M. A. Ivanov, M. A. Kreslavsky, S. Pratt, and B. J. Thomson (1999), Possible ancient oceans on Mars: Evidence from Mars Orbiter Laser Altimeter data, *Science*, *286*(5447), 2134–2137, doi:10.1126/science.286.5447.2134.

Heller, P. L., and C. Paola (1996), Downstream changes in alluvial architecture: An exploration of controls on channel-stacking patterns, *J. Sediment. Res.*, *66*(2), 297–306.

Irwin, R. P., and J. R. Zimbelman (2012), Morphometry of Great Basin pluvial shore landforms: Implications for paleolake basins on Mars, *J. Geophys. Res.*, *117*, E07004, doi:10.1029/2012je004046.

Irwin, R. P., A. D. Howard, R. A. Craddock, and J. M. Moore (2005), An intense terminal epoch of widespread fluvial activity on early Mars: 2. Increased runoff and paleolake development, *J. Geophys. Res.*, *110*, E12S15, doi:10.1029/2005je002460.

Ivanov, M. A., and J. W. Head (2001), Chryse Planitia, Mars: Topographic configuration, outflow channel continuity and sequence, and tests for hypothesized ancient bodies of water using Mars Orbiter Laser Altimeter (MOLA) data, *J. Geophys. Res.*, *106*(E2), 3275–3295, doi:10.1029/2000je001257.

Jerolmack, D. J. (2009), Conceptual framework for assessing the response of delta channel networks to Holocene sea level rise, *Quat. Sci. Rev*, *28*(17-18), 1786–1800, doi:10.1016/j.quascirev.2009.02.015.

Jerolmack, D. J., D. Mohrig, M. T. Zuber, and S. Byrne (2004), A minimum time for the formation of Holden Northeast fan, Mars, *Geophys. Res. Lett.*, *31*, L21701, doi:10.1029/2004gl021326.

Kerber, L., and J. W. Head (2010), The age of the Medusae Fossae Formation: Evidence of Hesperian emplacement from crater morphology, stratigraphy, and ancient lava contacts, *Icarus*, *206*(2), 669–684, doi:10.1016/j.icarus.2009.10.001.

Kerber, L., J. W. Head, J. B. Madeleine, F. Forget, and L. Wilson (2011), The dispersal of pyroclasts from Apollinaris Patera, Mars: Implications for the origin of the Medusae Fossae Formation, *Icarus*, *216*(1), 212–220, doi:10.1016/j.icarus.2011.07.035.

Kirk, R. L., et al. (2008), Ultrahigh resolution topographic mapping of Mars with MRO HiRISE stereo images: Meter-scale slopes of candidate Phoenix landing sites, *J. Geophys. Res.*, *113*, E00A24, doi:10.1029/2007je003000.

Kneller, B., and C. Buckee (2000), The structure and fluid mechanics of turbidity currents: A review of some recent studies and their geological implications, *Sedimentology*, *47*, 62–94, doi:10.1046/j.1365-3091.2000.047s1062.x.

Lamb, M. P., T. Hickson, J. G. Marr, B. Sheets, C. Paola, and G. Parker (2004), Surging versus continuous turbidity currents: Flow dynamics and deposits in an experimental intraslope minibasin, *J. Sediment. Res.*, *74*(1), 148–155, doi:10.1306/062103740148.

Lamb, M. P., J. Nittrouer, D. Mohrig, and J. Shaw (2012), Backwater and river-plume controls on scour upstream of river mouths: Implications for fluvio-deltaic morphodynamics, *J. Geophys. Res.*, *117*, F01002, doi:10.1029/2011JF002079.

Lefort, A., D. M. Burr, R. A. Beyer, and A. D. Howard (2012), Inverted fluvial features in the Aeolis-Zephyria Plana, western Medusae Fossae Formation, Mars: Evidence for post-formation modification, *J. Geophys. Res.*, *117*, E03007, doi:10.1029/2011je004008.

Lewis, K. W., and O. Aharonson (2006), Stratigraphic analysis of the distributary fan in Eberswalde crater using stereo imagery, *J. Geophys. Res.*, *111*, E06001, doi:10.1029/2005je002558.

Lewis, K. W., O. Aharonson, J. P. Grotzinger, R. L. Kirk, A. S. McEwen, and T. A. Suer (2008), Quasi-periodic bedding in the sedimentary rock record of Mars, *Science*, *322*(5907), 1532–1535, doi:10.1126/science.1161870.

Limaye, A. B. S., O. Aharonson, and J. T. Perron (2012), Detailed stratigraphy and bed thickness of the Mars north and south polar layered deposits, *J. Geophys. Res.*, *117*, E06009, doi:10.1029/2011je003961.

Lucchitta, B. K., H. M. Ferguson, and C. Summers (1986), Sedimentary deposits in the northern lowland plains, Mars, *Proc. Lunar Planet. Sci. Conf. 17th*, Part 1, *J. Geophys. Res.*, *91*, suppl., E166–E174, doi:10.1029/JB091iB13p0E166.

Malin, M. C., and K. S. Edgett (1999), Oceans or seas in the Martian northern lowlands: High resolution imaging tests of proposed coastlines, *Geophys. Res. Lett.*, *26*(19), 3049–3052, doi:10.1029/1999gl002342.

Malin, M. C., and K. S. Edgett (2000), Sedimentary rocks of early Mars, *Science*, *290*(5498), 1927–1937, doi:10.1126/science.290.5498.1927.

Malin, M. C., and K. S. Edgett (2001), Mars Global Surveyor Mars Orbiter Camera: Interplanetary cruise through primary mission, *J. Geophys. Res.*, *106*(E10), 23,429–23,570, doi:10.1029/2000je001455.

Malin, M. C., and K. S. Edgett (2003), Evidence for persistent flow and aqueous sedimentation on early Mars, *Science*, *302*(5652), 1931–1934, doi:10.1126/science.1090544.

Malin, M. C., et al (2007), Context Camera Investigation on board the Mars Reconnaissance Orbiter, *J. Geophys. Res.*, *112*, E05S04, doi:10.1029/2006JE002808.

Mandt, K. E., S. L. de Silva, J. R. Zimbelman, and D. A. Crown (2008), Origin of the Medusae Fossae Formation, Mars: Insights from a synoptic approach, *J. Geophys. Res.*, *113*, E12011, doi:10.1029/2008je003076.

Mangold, N., E. S. Kite, M. G. Kleinhans, H. Newsom, V. Ansan, E. Hauber, E. Kraal, C. Quantin, and K. Tanaka (2012), The origin and timing of fluvial activity at Eberswalde crater, Mars, *Icarus*, *220*(2), 530–551, doi:10.1016/j.icarus.2012.05.026.

Martinez, J. L. C., L. C. Perez, A. Marcuello, P. A. Cazo, M. M. Carpio, and F. Bellmunt (2010), Exhumed channel sandstone networks within fluvial fan deposits from the Oligo-Miocene Caspe Formation, South-east Ebro Basin (North-east Spain), *Sedimentology*, *57*(1), 162–189, doi:10.1111/j.1365-3091.2009.01096.x.

McEwen, A. S., et al. (2007), Mars reconnaissance orbiter's high resolution imaging science experiment (HiRISE), *J. Geophys. Res.*, *112*, E05S02, doi:10.1029/2005JE002605.

Metz, J. M., J. P. Grotzinger, D. Mohrig, R. Milliken, B. Prather, C. Pirmez, A. S. McEwen, and C. M. Weitz (2009), Sublacustrine depositional fans in southwest Melas Chasma, *J. Geophys. Res.*, *114*, E10002, doi:10.1029/2009je003365.

Meyer-Peter, E., and R. Müller (1948), Formulas for bed-load transport, in *Proceedings of the 2nd Meeting of the International Association of Hydraulic Structures Research*, pp. 39–64, Stockholm, Sweden.

Mohrig, D., P. L. Heller, C. Paola, and W. J. Lyons (2000), Interpreting avulsion process from ancient alluvial sequences: Guadalope-Matarranya system (northern Spain) and Wasatch Formation (western Colorado), *Geol. Soc. Am. Bull.*, *112*(12), 1787–1803, doi:10.1130/0016-7606(2000)112<1787:iapfaa>2.0.co;2.

Moore, J. M., A. D. Howard, W. E. Dietrich, and P. M. Schenk (2003), Martian layered fluvial deposits: Implications for Noachian climate scenarios, *Geophys. Res. Lett.*, *30*(24), 2292, doi:10.1029/2003gl019002.

Mouginot, J., A. Pommerol, W. Kofman, P. Beck, B. Schmitt, A. Herique, C. Grima, A. Safaeinili, and J. J. Plaut (2010), The 3-5 MHz global reflectivity map of Mars by MARSIS/Mars Express: Implications for the current inventory of subsurface H2O, *Icarus*, *210*(2), 612–625, doi:10.1016/j.icarus.2010.07.003.

Mouginot, J., A. Pommerol, P. Beck, W. Kofman, and S. M. Clifford (2012), Dielectric map of the Martian northern hemisphere and the nature of plain filling materials, *Geophys. Res. Lett.*, *39*, L02202, doi:10.1029/2011gl050286.

Newsom, H. E., G. E. Brittelle, C. A. Hibbitts, L. J. Crossey, and A. M. Kudo (1996), Impact crater lakes on Mars, *J. Geophys. Res.*, *101*(E6), 14,951–14,955, doi:10.1029/96je01139.

Newsom, H. E., et al. (2010), Inverted channel deposits on the floor of Miyamoto crater, Mars, *Icarus*, *205*(1), 64–72, doi:10.1016/j.icarus.2009.03.030.

Okubo, C. H. (2010), Structural geology of Amazonian-aged layered sedimentary deposits in southwest Candor Chasma, Mars, *Icarus*, *207*(1), 210–225, doi:10.1016/j.icarus.2009.11.012.

Pain, C. F., and C. D. Ollier (1995), Inversion of relief - A component of landscape evolution, *Geomorphology*, *12*(2), 151–165, doi:10.1016/0169-555x(94)00084-5.

Pain, C. F., J. D. A. Clarke, and M. Thomas (2007), Inversion of relief on Mars, *Icarus*, *190*(2), 478–491, doi:10.1016/j.icarus.2007.03.017.

Paola, C., P. L. Heller, and C. L. Angevine (1992), The large-scale dynamics of grain-size variation in alluvial basins, 1: Theory, *Basin Res.*, *4*(2), 73–90.

Parker, G. (1991), Selective sorting and abrasion of river gravel. 2. Applications, *J. Hydraul. Eng.*, *117*(2), 150–171, doi:10.1061/(asce)0733-9429(1991)117:2(150).

Parker, G. (2008), Transport of gravel and sediment mixtures, in *Sedimentation Engineering: Processes, Management, Modeling, and Practice*, edited by M. H. Garcia, pp., 165–251, Am. Soc. of Civ. Eng., Reston, Va.

Parker, T. J., R. S. Saunders, and D. M. Schneeberger (1989), Transitional morphology in west Deuteronilus Mensae, Mars - Implications for modification of the lowland upland boundary, *Icarus*, *82*(1), 111–145, doi:10.1016/0019-1035(89)90027-4.

Parker, T. J., D. S. Gorsline, R. S. Saunders, D. C. Pieri, and D. M. Schneeberger (1993), Coastal geomorphology of the Martian northern plains, *J. Geophys. Res.*, *98*(E6), 11,061–11,078, doi:10.1029/93je00618.

Parker, G., P. R. Wilcock, C. Paola, W. E. Dietrich, and J. Pitlick (2007), Physical basis for quasi-universal relations describing bankfull hydraulic geometry of single-thread gravel bed rivers, *J. Geophys. Res.*, *112*, F04005, doi:10.1029/2006jf000549.

Perron, J. T., J. X. Mitrovica, M. Manga, I. Matsuyama, and M. A. Richards (2007), Evidence for an ancient martian ocean in the topography of deformed shorelines, *Nature*, *447*(7146), 840–843, doi:10.1038/nature05873.

Potemkina, T. G. (2011), Sediment runoff formation trends of major tributaries of Lake Baikal in the 20th century and at the beginning of the 21st century, *Russ. Meteorol. Hydrol.*, *36*(12), 819–825, doi:10.3103/s1068373911120077.

Prelat, A., J. A. Covault, D. M. Hodgson, A. Fildani, and S. S. Flint (2010), Intrinsic controls on the range of volumes, morphologies, and dimensions of submarine lobes, *Sediment. Geol.*, *232*(1-2), 66–76, doi:10.1016/j.sedgeo.2010.09.010.

Rhodes, D. D. (1980), Exhumed topography - A case study of the Stanislaus Table Mountain, California, *NASA Tech. Memo.*, *TM-82385*, 397–399.

Sagan, C., and G. Mullen (1972), Earth and Mars - Evolution of atmospheres and surface temperatures, *Science*, *177*(4043), 52–56, doi:10.1126/science.177.4043.52.

Schon, S. C., J. W. Head, and C. I. Fassett (2012), An overfilled lacustrine system and progradational delta in Jezero crater, Mars: Implications for Noachian climate, *Planet. Space Sci.*, *67*(1), 28–45, doi:10.1016/j.pss.2012.02.003.

Scott, D. H., and K. L. Tanaka (1986), Geologic map of the western equatorial region of Mars, *U.S. Geol. Surv. Misc. Invest.*, Map I-1802-A, 1:15,000,000.

Sharp, R. P. (1973), Mars - Fretted and chaotic terrains, *J. Geophys. Res.*, *78*(20), 4073–4083, doi:10.1029/JB078i020p04073.

Sharp, R. P., and M. C. Malin (1975), Channels on Mars, *Geol. Soc. Am. Bull.*, *86*, 593–609.

Slingerland, R., and N. D. Smith (2004), River avulsions and their deposits, *Annu. Rev. Earth Planet. Sci.*, *32*, 257–285, doi:10.1146/annurev.earth.32.101802.120201.

Smith, D. E., et al. (2001), Mars Orbiter Laser Altimeter: Experiment summary after the first year of global mapping of Mars, *J. Geophys. Res.*, *106*(E10), 23,689–23,722, doi:10.1029/2000je001364.

Tanaka, K. L., J. A. Skinner, and T. M. Hare (2005), Geologic map of the northern plains of Mars, *U.S. Geol. Surv. Sci. Invest. Map, 2888*.

Van Kranendonk, M. J. (2006), Volcanic degassing, hydrothermal circulation and the flourishing of early life on Earth: A review of the evidence from c. 3490-3240 Ma rocks of the Pilbara Supergroup, Pilbara Craton, Western Australia, *Earth Sci. Rev.*, *74*(3-4), 197–240, doi:10.1016/j.earscirev.2005.09.005.

Watters, T. R., et al. (2007), Radar sounding of the Medusae Fossae Formation Mars: Equatorial ice or dry, low-density deposits?, *Science*, *318*(5853), 1125–1128, doi:10.1126/science.1148112.

Williams, R. M. E., R. P. Irwin, and J. R. Zimbelman (2009), Evaluation of paleohydrologic models for terrestrial inverted channels: Implications for application to martian sinuous ridges, *Geomorphology*, *107*(3-4), 300–315, doi:10.1016/j.geomorph.2008.12.015.

Wood, L. J. (2006), Quantitative geomorphology of the Mars Eberswalde delta, *Geol. Soc. Am. Bull.*, *118*(5-6), 557–566, doi:10.1130/b25822.1.

Zimbelman, J. R., and L. J. Griffin (2010), HiRISE images of yardangs and sinuous ridges in the lower member of the Medusae Fossae Formation, Mars, *Icarus*, *205*(1), 198–210, doi:10.1016/j.icarus.2009.04.003.

Zimbelman, J. R., and S. P. Scheidt (2012), Hesperian age for western Medusae Fossae Formation, Mars, *Science*, *336*(6089), 1683–1683, doi:10.1126/science.1221094.